Keith E. Knipling, David C. Dunand, David N. Seidman
Department of Materials Science and Engineering Northwestern University, Evanston, USA

Criteria for developing castable, creep-resistant aluminum-based alloys – A review

Dedicated to Professor Dr. Gernot Kostorz on the occasion of his 65th birthday

We describe four criteria for the selection of alloying elements capable of producing castable, precipitation-strengthened Al alloys with high-temperature stability and strength: these alloying elements must (i) be capable of forming a suitable strengthening phase, (ii) show low solid solubility in Al, (iii) low diffusivity in Al, and (iv) retain the ability for the alloy to be conventionally solidified. With regard to criterion (i), we consider those systems forming Al_3M trialuminide compounds with a cubic $L1_2$ crystal structure, which are chemically and structurally analogous to Ni_3Al in the Ni-based superalloys. Eight elements, clustered in the same region of the periodic table, fulfill criterion (i): the first Group 3 transition metal (Sc), the three Group 4 transition metals (Ti, Zr, Hf) and the four latest lanthanide elements (Er, Tm, Yb, Lu). Based on a review of the existing literature, these elements are assessed in terms of criteria (ii) and (iii), which satisfy the need for a dispersion in Al with slow coarsening kinetics, and criterion (iv), which is discussed based on the binary phase diagrams.

Keywords: Aluminum alloys; Trialuminides; Precipitation strengthening; Creep

1. Introduction

Improved strength at elevated temperatures has been a continuing goal in aluminum alloy development for more than three decades (see e. g. [1–3] or a number of papers in [4]). Aluminum-based alloys have several characteristics that make them especially attractive for the development of high-temperature, high-strength alloys. As with the Ni-based superalloys, the unit cell of Al is face-centered cubic (fcc), whose close-packed structure is more creep resistant than more open crystalline structures. Moreover, Al alloys are naturally oxidation resistant due to an extremely stable passivating protective oxide layer. For weight-sensitive applications, the low density of Al alloys allows for materials with high specific strengths. Finally, Al alloys are considerably more economical than existing high-temperature aerospace (e. g. Ni- and Ti-based) alloys.

Historically, most efforts to develop high-strength, thermally-stable Al alloys have sought alloying elements that exhibit both limited solid solubility and low diffusivity in Al. This approach was originally promoted by Adam [2] who argued, based on diffusion-controlled coarsening theory, that dispersed phases formed from such alloying additions would be resistant to Ostwald ripening. Borne out of these ideas are the rapidly-solidified alloys based on the eutectic Al–Fe system that, to date, represent the most promising high-temperature Al-based alloys. These include the well-known Al–Fe–V–Si alloys developed by Skinner et al. [5–7], as well as more complex Al–Fe based systems with ternary and often quaternary additions such as Ce, Ni, Co, Zr, Mo, V [2, 3, 8–10]. These alloys, however, derive their high-temperature strength from a large volume fraction of stable precipitates that form directly from the melt during rapid solidification.

A conventional ingot metallurgy approach to alloy development offers several benefits, both from performance and economic standpoints. Aluminum alloys compacted from powders produced, for example, by rapid solidification processing (RSP) and mechanical alloying (MA) are prone to brittleness, in part due to residual porosity and the presence of oxides from the original powders. Also, the powder production and subsequent compaction stages negatively impact the commercial competitiveness of these alloys. More importantly, solid-state precipitation during post-solidification aging offers the potential for generating a much finer dispersion of strengthening phases than those formed in the melt.

This review considers the general requirements – and challenges – for developing such a castable, precipitation-strengthened, thermally-stable Al-based alloy. The current work is distinguished from other reviews, most notably by Starke and colleagues [11–13], devoted to the intelligent *design* of high-strength aluminum alloys. This work is concerned less with design, but rather focuses on four broad criteria that a suitable alloying addition to Al must meet. Specifically, we seek alloying additions that are (i) capable of forming a trialuminide strengthening phase, exhibit (ii) low solid solubility and (iii) low diffusivity in Al, and (iv) retain the ability for the alloy to be conventionally solidified.

1.1. General strengthening requirements for high-strength, high-temperature alloys

1.1.1. Physical metallurgy of Ni-based and Al-based alloys

Before discussing the challenges of developing high-strength, high-temperature Al alloys, it is valuable to con-

sider what are certainly the most complex and successfully engineered high-temperature alloys developed to date – the Ni-based superalloys. Modern Ni-based superalloys are able to sustain stresses of the order of 150 MPa for thousands of hours, operating at temperatures ca. $0.75T_m$. This extraordinary creep resistance is achieved primarily by additions of Al to produce ordered Ni_3Al precipitates (γ'), with the $L1_2$ structure, which are both isomorphous and coherent with the fcc Ni-rich matrix (γ). The solubility in Ni of γ'-producing Al is substantial, thus allowing for very large volume fractions of precipitated γ' which, in many commercial alloys, exceeds 70 vol.%.

Development of Al alloys by conventional solidification processing is subject to the restriction that appreciable solubility (> 1 at.%) at equilibrium is limited to eight alloying elements – Zn, Ag, Mg, Li, Ga, Ge, Cu, Si (in order of decreasing maximum solubility) – which are situated near Al in the periodic table [14–17]. This limitation necessarily restricts the equilibrium volume fraction of any precipitated phase (excluding those for the above elements of which only Ag, Mg, Li, and Cu form stable intermetallic compounds with Al) to a value that is less than 1 vol.%, which is one to two orders of magnitude smaller than typically found in Ni-based superalloys.

1.1.2. Precipitation strengthening mechanisms

To appreciate the ramifications of the generally very limited solid solubility of alloying elements in Al (and the concomitantly low volume fraction of the dispersed phase), it is necessary to consider the quantitative effect of precipitate volume fraction on the predicted strengthening increment in precipitation-strengthened alloys. The strengthening produced by the interaction of dislocations with a dispersion of incoherent, inpenetrable particles within a matrix phase was first described by Orowan [18], and has been reviewed thoroughly (e. g., [19–24]). The shear stress required for a dislocation to loop around a precipitate is inversely proportional to the edge-to-edge distance between precipitates, and the increase in yield strength $\Delta\sigma_{or}$ due to this mechanism is given by [25]:

$$\Delta\sigma_{or} = M \cdot \frac{0.4 \cdot Gb}{\pi\sqrt{(1-\nu)}} \cdot \frac{\ln\left(\frac{2\bar{R}}{b}\right)}{\lambda} \tag{1}$$

where M is the Taylor factor for the matrix, G and ν are the shear modulus and Poisson ratio of the matrix, b is the magnitude of the Burgers vector, $\bar{R}$ is the mean planar precipitate radius (not equal to the mean radius, $\langle R\rangle$), and λ is an effective inter-precipitate distance, which takes into account the finite size of the precipitates. Both $\bar{R}$ and λ depend on the distribution of precipitate sizes. For a monodispersed assembly, these parameters are given by [20, 22, 23]:

$$\bar{R} = \frac{\pi}{4}\langle R\rangle \tag{2}$$

and

$$\lambda = \left(\sqrt{\frac{2\pi}{3f}} - 2\frac{\pi}{4}\right)\langle R\rangle \tag{3}$$

where f is the precipitate volume fraction. Equations (2) and (3) are also good approximations for polydispersed arrays [23].

A plot of Orowan stress as a function of precipitate radius for different volume fractions, generated using Eq. (1), is displayed in Fig. 1 with parameters pertinent to Al: M = 3.06 [26], b = 0.286 nm [27], G = 25.4 GPa [27], and ν = 0.345 [26]. Because of the intrinsically low precipitate volume fraction in Al-based alloys, it is critical that these dispersed phases be small (of the order of 10 nm or less) and remain small (resist coarsening) throughout thermal exposure during operation. This requirement does not apply to Ni-based superalloys, given their much higher solubility for different alloying elements, thus allowing for higher volume fractions of the ordered strengthening phase, γ'. Also, the higher shear modulus of Ni (G = 78.9 GPa [27]) increases the disparity in Orowan stresses between Ni-based and Al-based alloys.

The strengthening mechanisms are also somewhat different in coarse-grained Ni- and Al-based alloys, as might be anticipated on account of the large disparity in precipitate volume fraction, and in neither system is deformation at elevated temperature governed directly by the Orowan mechanism of dislocation looping. During creep deformation of Ni-based superalloys, dislocations are generally confined to the narrow γ channels between the large γ' precipitates, where complex dislocation networks form and inhibit further dislocation motion [28, 29]. In Al-based precipitation-strengthened alloys, sufficient thermal energy is usually available under creep conditions to allow glissile dislocations to circumvent coherent precipitates by climbing out of their glide plane. The increase in length of the dislocation during the climb process results in a threshold stress (which is linearly proportional to the Orowan stress [30–32]), below which creep deformation is not measurable. For coherent precipitates, elastic interactions due to precipitate–matrix modulus and lattice parameter mismatches can further increase the creep threshold stress

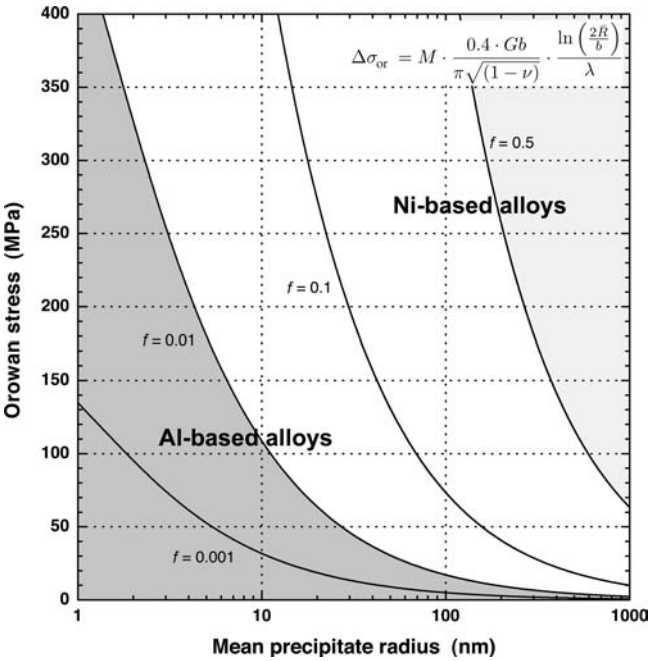

Fig. 1. The Orowan stress, Eq. (1), as a function of mean precipitate radius, $\langle R\rangle$, for various volume fractions, f, of dispersed phase.

[33]. These elastic interactions generally result in an optimum precipitate size for creep resistance, whereas dislocation climb predicts that alloys with the smallest precipitates have the greatest threshold stress (since it is proportional to the Orowan stress), provided precipitates are not sheared. Nevertheless, the comparison in Fig. 1 shows the critical need for very fine, and thus very coarsening-resistant, precipitates in Al alloys to compensate for the intrinsically limited volume fraction obtained during conventional casting of these alloys.

1.1.3. Precipitate stability

Ostwald ripening (coarsening) occurs during the latest stages of precipitation and involves the growth of larger precipitates at the expense of smaller ones. The kinetics of this process are controlled by volume diffusion, as solute atoms are transferred through the matrix from the shrinking precipitates to the growing ones, if the evaporation-condensation model obtains. In their classic work on the coarsening of a binary alloy, Lifshitz and Slyozov [34] and Wagner [35] (LSW) showed that the average precipitate size $\langle R \rangle$ increases with time t according to:

$$\langle R(t) \rangle^3 - \langle R(t=0) \rangle^3 = kt \tag{4}$$

where $\langle R(t) \rangle$ is the average precipitate radius at time t, $\langle R(t=0) \rangle$ is the average initial precipitate radius at the onset of coarsening, and k is the rate constant given by [36]:

$$k \propto \frac{D\sigma}{(C_e^{\beta} - C_e^{\alpha})^2} \tag{5}$$

Here, D is the diffusivity of the rate-controlling solute, σ is the precipitate–matrix interfacial free energy, and C_e^{β} and C_e^{α} are the equilibrium solubilities (assuming a planar interface) of the solute species in the precipitate and matrix phases, respectively.

For any creep-resistant alloy, it is essential that the dispersion of precipitates resists coarsening during prolonged exposure at elevated service temperatures. As indicated in Fig. 1, this requirement is especially imperative for Al-based alloys because of the generally limited solubility of most solutes in Al and the concomitant limited volume fractions ($f < 0.01$) of dispersed phases.

1.2. Summary

Based on the behavior of modern Ni-based superalloys, which remain mechanically strong at temperatures exceeding 75 % of their absolute melting temperature, it is conceivable that Al-based alloys could be analogously developed that would be useful to 425 °C (0.75 T_m). The creep resistance of Ni-based superalloys is conferred by very large volume fractions of the precipitated Ni_3Al ordered phase (γ'), the $L1_2$ structure. An effective high-temperature Al alloy should thus exhibit a similar structural constitution, with suitable alloying additions to Al exhibiting the following qualities:

(i) **Capability of forming strengthening intermetallic phases.** As is true for γ' in the Ni-based systems, a high-temperature Al alloy should contain a large volume fraction of a suitable dispersed phase, which must be thermodynamically stable and difficult to shear by dislocations at the intended service temperature. These precipitated phases should also exhibit a similar crystal structure to, and a low lattice parameter mismatch with, the Al solid solution.

(ii) **Low solid solubility in Al.** A low equilibrium solid solubility at the intended service temperature is necessary to retard volume diffusion-controlled coarsening (Eq. (5)) and prevent dissolution of the precipitated phases. By the lever rule, limited solid solubility also maximizes the equilibrium volume fraction of the dispersed phase.

(iii) **Low diffusivity in Al.** Limited diffusivity of the solutes in Al should also stifle volume diffusion-controlled coarsening (Eq. (5)), allowing the precipitates to remain effective barriers to dislocation motion at elevated temperatures.

(iv) **Ability to be conventionally cast.** This review is concerned with developing Al alloys via standard ingot metallurgy processing routes, and therefore the alloy must be amenable to conventional casting.

In the following Sections, we systematically evaluate potential alloying additions to Al with respect to each of the above four criteria.

2. Selection criteria for castable precipitation-strengthened alloys

2.1. Capability of forming strengthening intermetallic phases

The first criterion stated requires that any suitable system must have the capability to form a fine dispersion of a secondary strengthening phase. As suggested by Fine et al. [1, 37, 38], intermetallic compounds formed with Al are the most promising candidates for strengthening phases in ductile, thermally-stable dispersion-strengthened Al-based alloys. While a number of potential Al-rich intermetallics can be used to strengthen Al [39], trialuminide compounds of the type Al_3M (where M is an element of the transition metals, lanthanide, or actinide series) have particularly attractive characteristics that include low density (they are nominally 75 % Al on an atomic basis), high specific strength, good thermal stability (they have generally very high melting points), and excellent oxidation resistance (again, mostly due to the high Al content). Moreover, the trialuminides are directly analogous, in terms of chemistry, to the γ' Ni_3Al ($L1_2$) ordered precipitates in the Ni-based alloys.

Extending the Ni-based alloy analogy further, it is desirable that these dispersed trialuminide precipitates have the cubic $L1_2$ structure. The similarity in crystal structure between the matrix and precipitated phases allows for a coherent interface between the two phases which, in turn, maximizes the strengthening efficacy of the dispersed phase (e. g., by allowing for elastic interactions between dislocations and misfitting precipitates). Furthermore, coherency minimizes the surface energy per unit area of the heterophase interface, conferring stability at high temperatures by reducing the driving force for precipitate coarsening; that is, the excess free energy associated with the total interfacial area between the precipitate phase and the matrix.

A review of the published phase diagrams and crystallographic data [40–42] indicates that a number of alloying

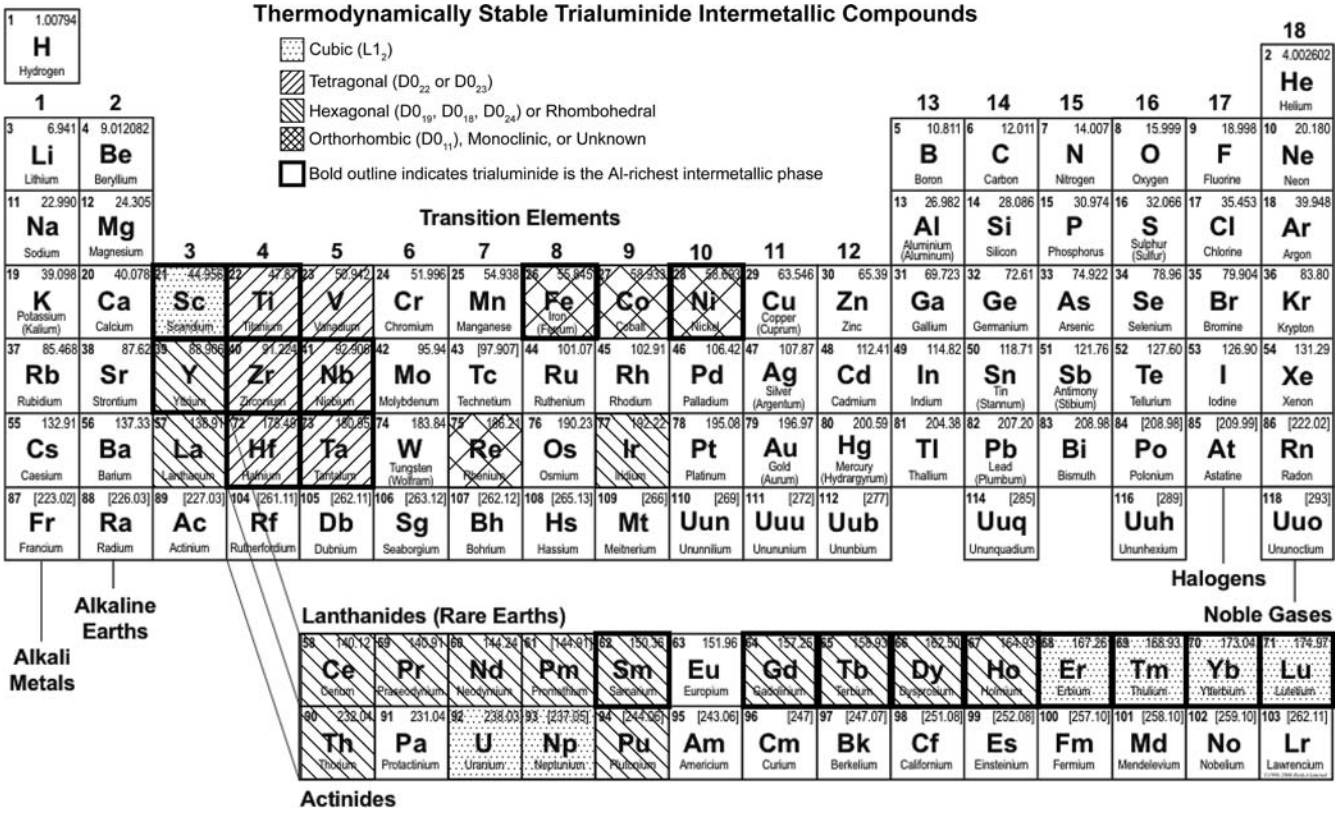

Fig. 2. Alloying additions to Al which form thermodynamically stable trialuminide (Al_3M) intermetallic compounds, with the equilibrium structure indicated.

additions crystallize to form stable Al_3M trialuminides, as shown graphically in the periodic table of Fig. 2. The high-symmetry cubic $L1_2$ and related tetragonal $D0_{22}$ and $D0_{23}$ structures are prevalent among the early transition elements (Groups 3 to 5), with other lower-symmetry structures obtained with a few of the transition elements of later groups (Fe, Co, Ni, Re, Ir). Trialuminide intermetallic compounds are even more abundant among the lanthanide (rare earth, RE) elements; with the exception of Eu, all RE elements form thermodynamically stable Al_3RE compounds. This is also the case for several of the early actinide elements (Th, U, Np, Pu). We note that other metastable Al_3M trialuminides also exist, e. g. Al_3Li, which is a potent strengthening phase in aerospace Al-based alloys, but they are not discussed further since their metastability does not fulfill the criterion of high-temperature stability. They may, however, find use as ternary (or higher order) alloying additions in Al–M systems exhibiting stable Al_3M trialuminides.

2.1.1. Trialuminides formed from the transition elements

Of the only seven thermodynamically stable $L1_2$ trialuminides (Fig. 2), Al_3Sc has generated by far the most attention in the scientific literature (see Royset and Ryum [43] for a comprehensive review of the role of Al_3Sc in Al alloys). Besides Al_3Sc, no other thermodynamically stable $L1_2$ trialuminides exist among the transition elements.

Just below Sc in the periodic table is Y, which forms an Al_3Y trialuminide with an equilibrium hexagonal $D0_{19}$ (Ni_3Sn-type) structure. In rapidly-solidified hypereutectic alloys, however, Foley et al. [44] reported the existence of a metastable cubic $L1_2$ Al_3Y phase that formed during solidification.

Also near to Sc are the Group 4 (Ti, Zr, Hf) and Group 5 (V, Nb, Ta) elements, which crystallize with the body-centered tetragonal $D0_{22}$ (or $D0_{23}$ for Al_3Zr) structures. In their monolithic form, these trialuminides have received considerable attention as potential high-strength, high-temperature structural materials, most notably Al_3Ti since it is the least dense of this class ($3.36\ g \cdot cm^{-3}$) [45–49]. Unfortunately, however, the low-symmetry tetragonal structure makes these phases intrinsically brittle. The $D0_{22}$ and $D0_{23}$ structures are, however, closely related to the cubic $L1_2$ structure (Fig. 3) and much effort has concentrated on alloying these binary intermetallics to transform them to the higher-symmetry $L1_2$ structure, in the hope that the increased number of independent slip systems will improve toughness. For example, Al_3Ti ($D0_{22}$) can be transformed to the cubic $L1_2$ structure by alloying with late fourth-period transition elements such as Cr, Mn, Fe, Co, Ni, Cu, or Zn [47, 50–60]. Similarly, Li, Cr, Mn, Fe, Ni, and Cu have been added to Al_3Zr to increase the stability of the cubic $L1_2$ structure [61–63], and Cu and Zn have also been shown to stabilize the $L1_2$ structure of Al_3Hf [64].

Carlsson and Meschter [65] and Xu and Freeman [66, 67] have shown by *ab initio* calculations that the stability of the $D0_{22}/D0_{23}$ structure relative to the $L1_2$ increases rapidly as the transition metal d-electron count increases. Therefore, the likelihood of transforming the stable tetragonal structure to a metastable cubic $L1_2$ phase is greater for the Group 4 (Ti, Zr, Hf) elements than it is for the Group 5 (V, Nb, Ta). Indeed, while Al_3Ti and Al_3Zr have been successfully stabilized into the $L1_2$ structure by alloying additions

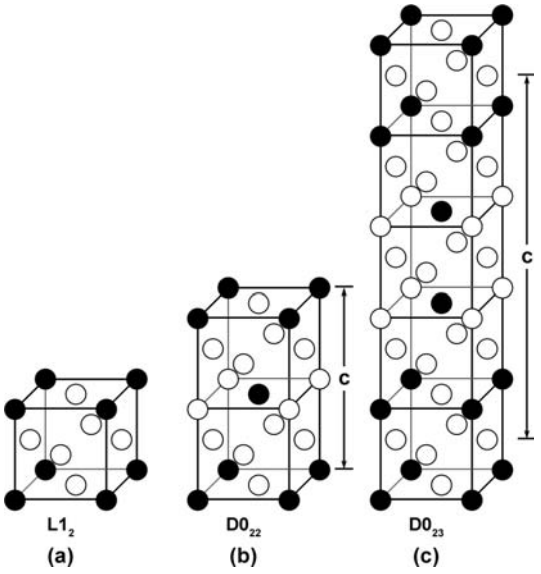

Fig. 3. The (a) $L1_2$, (b) $D0_{22}$, and (c) $D0_{23}$ structures. Adapted from Yamaguchi [45].

of late fourth-period transition elements, similar efforts to produce cubic $L1_2$ Group 5 trialuminides, such as Al_3Nb and Al_3Ta, have proven unsuccessful [47, 687].

Since the free energy difference between the equilibrium and metastable structures is so small, one might expect the $L1_2$ structure of the Group 4 trialuminides (Al_3Ti, Al_3Zr, Al_3Hf) to be readily achievable when precipitated from solid solution. Indeed, the decomposition sequence during aging of supersaturated Al–Ti [69–74], Al–Zr [14, 75–83], and Al–Hf [84–92] solid solutions has been reported to occur firstly by the formation of a metastable cubic $L1_2$ Al_3M phase, with prolonged exposure (hundreds of hours) at high temperatures (> 450 °C) required before this phase transforms to the equilibrium tetragonal Al_3M structure. Furthermore, single phase $L1_2$-structured Group 4 transition metal trialuminides (Al_3Ti, Al_3Zr, Al_3Hf) have been produced through mechanical alloying, which do not transform to their respective equilibrium tetragonal structures until after heating at very high temperatures (485 °C, 550 °C, and 750 °C for Al_3Ti, Al_3Zr, and Al_3Hf, respectively) [93].

The Group 4 cubic $L1_2$ trialuminides, while thermodynamically metastable, readily precipitate from supersaturated solid solutions and are kinetically stable at temperatures well in excess of 400 °C. These transition elements are also extraordinarily slow diffusers in Al, as discussed below, and therefore show considerable promise as thermally stable secondary phases in precipitation-strengthened, high-temperature Al-based alloys.

2.1.2. Trialuminides formed from elements of the lanthanide series

There is a monotonic decrease in the radius of the rare earth atos across the lanthanide period, and this variation in atomic radius has been shown to influence strongly the stability, structure, and composition of the intermetallic compounds formed in the Al–RE systems [94–97]. With decreasing RE atomic radius, the structure of the corresponding trialuminide compound exhibits progressively more cubic character [94–96]. For larger metallic radii (Z = 57–64: La, Ce, Pr, Nd, Pm[1], Sm, or Gd), the hexagonal $D0_{19}$ structure (Ni_3Sn-type) is found. Those elements of intermediate size (Z = 65–67: Tb, Dy, Ho) possess rhombohedral and hexagonal (Ba_3Pb-, Ni_3Ti-, and Al_3Ho-type, respectively) structures in which cubic and hexagonal stacking is mixed. For the smallest radius RE atoms (Z = 68–71: Er, Tm, Yb, Lu) the cubic $L1_2$ (Cu_3Au-type) structure is observed.

The composition of the terminal Al-rich intermetallic phase is also strongly dependent on the atomic radius of the RE addition. On traversing the lanthanide period from Ce (Z = 58) to Lu (Z = 71), there is a transition in the most Al-rich intermetallic phase from $Al_{11}RE_3$ (also referred to as Al_4RE by some authors), being stable for early elements of the period, to Al_3RE which is stable for the late lanthanides. According to the published equilibrium phase diagrams [40–42], Al_3RE is the terminal intermetallic compound for the smaller lanthanide elements beyond Sm (Z = 62), inclusive. The trialuminide phases of the early, larger lanthanide series (Ce (Z = 58) to Pm (Z = 61)), therefore, are not in equilibrium with α-Al and hence may be not precipitated during aging.

The point at which this transition in composition of the Al-rich intermetallic phase occurs has been disputed, however [97]. In the Al-Gd system, for example, Al_3Gd is the equilibrium terminal intermetallic but Savage et al. [97, 98] report the stabilization of $Al_4Gd/Al_{11}Gd_3$ at high cooling rates during solidification. The existence of a metastable $Al_4Y/Al_{11}Y_3$ phase has similarly been reported in the as-cast structure of rapidly-solidified Al–Y alloys [99, 100], even though Al_3Y is the equilibrium terminal phase.

The transition in trialuminide structure from hexagonal/orthorhombic to cubic is also rather sensitive to small perturbations. Figure 2, which displays the equilibrium structures, indicates that thermodynamically stable cubic $L1_2$ structures are obtained for RE additions of Er (Z = 68) and beyond. Cannon and Hall [95], however, showed that applied pressure produced a structural transformation toward the more cubic structure in the lanthanide trialuminides, and obtained cubic $L1_2$ structures for Al_3Ho and Al_3Dy through such a pressure-induced polymorphic change. Conversely, impurities of Si may stabilize a non-equilibrium, rhom bohedral (Al_3Ho-type) structure for Al_3Er [40, 101].

2.1.3. Trialuminides formed from elements of the actinide series

We finally consider the trialuminides of the actinide series, of which there are four equilibrium Al_3M phases (Al_3Th, Al_3U, Al_3Np, Al_3Pu) as indicated in Fig. 2. Of particular interest are Al_3U and Al_3Np, which form thermodynamically stable cubic $L1_2$ structures. None of the actinide trialuminides, however, are in terminal equilibrium with their respective α-Al solid solutions [40, 41], and, therefore cannot be precipitated from α-Al during aging. While actinide metals could be considered as ternary elements to modify other Al_3M phases, their radioactive nature prevents practical engineering applications.

[1] The Al–Pm system is not well known, but is assumed to be similar to Al–Nd [40].

2.1.4. Lattice parameters of the cubic and tetragonal trialuminide phases

A small lattice parameter mismatch between the precipitate and matrix is essential for minimizing the interfacial free energy driving Ostwald ripening (Eq. (5)) and for maintaining a coherent and coplanar heterophase interface between the two phases [1, 37, 38, 83]. It is therefore useful to compare the lattice parameters, *a*, among the cubic $L1_2$ trialuminides in Fig. 2, as displayed in Table 1. For the Group 4 (Ti, Zr, Hf) and Group 5 (V, Nb, Ta) elements that form metastable cubic $L1_2$ trialuminides, data for the related equilibrium tetragonal $D0_{22}$ and $D0_{23}$ structures are also provided. The absolute lattice parameter mismatch, δ, for the cubic $L1_2$ structures is:

$$\delta = 100\left|1 - \frac{a}{a_0}\right| \tag{6}$$

Table 1. Reported lattice parameters and the corresponding mismatch with Al for cubic ($L1_2$) and related tetragonal ($D0_{22}$ or $D0_{23}$) Al_3M trialuminide intermetallic compounds.

Phase	Structure	Lattice parameters (Å)	Mismatch with Al	Absolute mismatch, δ	References
Group 3 transition elements					
Al_3Sc	$L1_2$	a = 4.103	+ 1.32 %	1.32 %	[102]
Al_3Y	$L1_2$[a]	a = 4.234	+ 4.55 %	4.55 %	[44]
Group 4 transition elements					
Al_3Ti	$L1_2$[a] $D0_{22}$	a = 3.967 a = 3.848 c = 8.596	− 2.04 % − 4.98 % + 6.13 %	2.04 % 5.36 %	[93] [39, 103]
Al_3Zr	$L1_2$[a] $D0_{23}$	a = 4.08 a = 4.014 c = 17.321	+0.75 % − 0.88 % + 6.92 %	0.75 % 2.89 %	[78, 93, 104] [39, 103]
Al_3Hf	$L1_2$[a] $D0_{22}$[b]	a = 4.048 a = 3.893 c = 8.925	− 0.04 % − 3.87 % + 10.20 %	0.04 % 5.98 %	[93] [105]
Group 5 transition elements					
Al_3V	$L1_2$[a,c] $D0_{22}$	a = 3.87 a = 3.780 c = 8.321	− 4.44 % − 6.66 % + 2.74 %	4.44 % 5.35 %	[67] [39, 103, 106]
Al_3Nb	$L1_2$[a] $L1_2$[a,c] $D0_{22}$	a = 4.11 a = 3.92 a = 3.844 c = 8.605	+ 1.49 % − 3.20 % − 5.08 % + 6.25 %	1.49 % 3.20 % 5.47 %	[39] [67] [39, 103]
Al_3Ta[d]	$D0_{22}$	a = 3.839 c = 8.535	− 5.20 % + 5.38 %	5.26 %	[103]
Lanthanide series (rare earths)					
Al_3Er	$L1_2$	a = 4.215	+ 4.08 %	4.08 %	[106 – 108]
Al_3Tm	$L1_2$	a = 4.203	+ 3.79 %	3.79 %	[106]
Al_3Yb	$L1_2$	a = 4.200	+ 3.71 %	3.71 %	[106]
Al_3Lu	$L1_2$	a = 4.187	+ 3.39 %	3.39 %	[106, 108]
Actinide series					
Al_3U	$L1_2$	a = 4.262	5.24 %	+ 5.24 %	[106]
Al_3Np	$L1_2$	a = 4.260	+ 5.20 %	5.20 %	[106]

[a] Metastable.
[b] Al_3Hf exists in two different crystallographic forms: a stable high temperature $D0_{23}$ phase and a stable low temperature $D0_{22}$ phase. The $D0_{23}$ structure is the one relevant to solid-state precipitation.
[c] Calculated [66].
[d] No reported metastable cubic $L1_2$ Al_3Ta.

where a_0 = 4.0496 Å is lattice parameter of Al. Taking into account the mismatch along both the *a*- and *c*-axes, the parameter δ for the tetragonal phases may be written as [37, 39, 92]:

$$\delta = \frac{100}{3}\left[2\left|1-\frac{a}{a_0}\right| + \left|1-\frac{c}{n\cdot a_0}\right|\right] \quad (7)$$

where $n = 2$ for $D0_{22}$ and $n = 4$ for $D0_{23}$.

The lattice parameters and corresponding mismatches displayed in Table 1 are published values for the *pure binary* Al_3M trialuminides measured at *room temperature*, which may be modified significantly by alloying or thermal expansion at elevated temperature.

The cubic and tetragonal phases in Table 1 are isostructural, respectively, and so there is generally extensive mutual solubility between them with a concomitant shift in lattice parameter, which is approximately linear with composition assuming Vegard's law obtains. Fine et al., for example, showed that the lattice parameters of both the stable ($D0_{23}$) and metastable ($L1_2$) Al_3Zr phases could be reduced by additions of Ti, Hf, or V [83, 109, 110]. The Al–Zr–V system, in particular, was studied extensively [83, 111–113], and the reduced lattice parameter mismatch was observed to decrease the rate of Ostwald ripening for both metastable cubic $L1_2$ and the equilibrium tetragonal $D0_{23}$ phases [37]. Similar improvements have been obtained in Al–Sc-based alloys, where partitioning of Zr to $Al_3(Sc_{1-x}Zr_x)$ [114–116] and Ti to $Al_3(Sc_{1-x}Ti_x)$ [117] has been shown to offer improved stability of the precipitated Al_3Sc-based trialuminides in dilute alloys compared to binary Al_3Sc [118]. These and other Group 3 (Y), Group 4 (Ti, Zr, Hf), and Group 5 (V, Nb, Ta) elements reduce the lattice parameter of Al_3Sc ($L1_2$) [119, 120], thus reducing the mismatch with Al. As discussed later, these ternary additions to the Al–Zr [83, 111–113] and Al–Sc [114–117] alloys are slower diffusers than either Zr or Sc, thus further improving coarsening resistance.

2.1.5. Summary

Trialuminide (Al_3M-type) intermetallic compounds have many beneficial characteristics including low density, high elastic modulus, high melting points, and are often stable with Al. They are therefore ideal dispersed strengthening phases for high-strength thermally-stable Al-based alloys. The cubic $L1_2$-structured trialuminides are especially attractive since these ordered fcc structures are commensurate with Al. While 31 elements form trialuminides when alloyed with Al, as shown in Fig. 2, only six elements – Sc, Er, Tm, Yb, Lu, U, and Np – form thermodynamically stable cubic $L1_2$ Al_3M structures. Several metastable $L1_2$ structures exist, most notably among the Group 4 and Group 5 elements. The Group 4 elements (Ti, Zr, Hf) are especially attractive since the degree of metastability of the cubic $L1_2$ trialuminide is very slight.

2.2. Solid solubility in α (Al)

Figure 4 shows the published phase diagrams of the Group 3 (Sc, Y, La), Group 4 (Ti, Zr, Hf), and Group 5 (V, Nb, Ta) transition elements alloyed with Al, positioned as they are situated in the periodic table. Many of the arguments we use for considering the capacity for precipitation strengthening (this Section) and also castability (Section 2.4) will be made with reference to features in the equilibrium binary phase diagrams. We discuss the particular features later, but a few patterns in Fig. 4 are worth commenting on now. The Group 3 (Sc, Y, La) elements exhibit terminal eutectics with Al, while the Group 4 (Ti, Zr, Hf) and Group 5 (V, Nb, Ta) are peritectics. Of the eutectic Group 3 elements, Sc is unique in that it exhibits the highest solid solubility and the lowest liquid solubility at the eutectic temperature. The other eutectic-forming elements, Y and La (as well as most of the lanthanides alloyed with Al), exhibit rather high liquid solubility of solute with very little solid solubility, as shown in Figs. 4b and 4c for Al–Y and Al–La, respectively. These features will have a profound influence on the conduciveness of the various systems for development into castable precipitation-strengthened alloys, as we discuss in detail later.

2.2.1. Requirements for precipitation strengthening

In the interest of precipitation-strengthening, a low solid solubility is desired to maximize the chemical driving force for nucleation and, concomitantly, the equilibrium volume fraction of the precipitated phase. Moreover, according to volume diffusion-controlled coarsening theory (Eq. (5)), limited solid solubility is also favorable for retarding Ostwald ripening of the precipitate dispersion, which is essential for creep resistance. As noted previously, appreciable solubility in Al exists only for eight elements (Zn, Ag, Mg, Li, Ga, Ge, Cu, Si) [14–17]. We therefore consider solid solubility primarily from the standpoint of a characteristic that maximizes the potential for precipitation strengthening.

The basic requirement for precipitation strengthening, as originally formulated in the seminal work of Merica et al. [124] to explain Wilm's serendipitous discovery of age hardening, is decreasing solute solubility with decreasing temperature. This criterion alone is not very useful since virtually all elements, when alloyed with Al, exhibit this behavior. A more discriminating feature by which to compare various systems, therefore, is to consider the potential for obtaining large volume fractions of dispersed phases which, as discussed in detail by Ryum [125], scales with the maximum solubility, C_{max}. This is exactly true only for eutectic systems as the liquid solubility of solute in peritectic systems is often the limiting factor for determining the amount of solute that may be quenched into solid solution. This point is discussed in more detail when considering castability.

A large maximum solubility, C_{max}, is also essential for solutionizing the alloys in the single phase α-Al solid solution prior to precipitation aging, which is necessary for achieving a homogenous distribution of supersaturated solute atoms after quenching, as well as a potential supersaturation of vacancies capable of accelerating precipitation. In addition to a large C_{max}, limited solubility at intermediate aging/service temperatures, say 400 °C (C_{400}), is favored for driving nucleation as well as retarding Ostwald ripening of the precipitated phase.

Finally, precipitation of an Al_3M trialuminide from solid solution requires that Al_3M is the most Al-rich intermetallic compound in the system (that is, Al_3M exists in equilibrium with the terminal α-Al solid solution). Several of the transition metals (V, Co, La, Ir), the early lanthanides (Ce, Pr, Nd,

Pm), and the actinides (Th, U, Np, Pu) all form trialuminides that are not the terminal intermetallic compound, and hence Al_3M may not be precipitated from solid solution in these systems.

Table 2 considers the cubic $L1_2$ Al_3M-forming systems in Fig. 2 with respect to the criteria favorable for precipitation strengthening. As indicated, all trialuminides except for Al_3V, Al_3U, and Al_3Np are in equilibrium with α-Al. Unfortunately, few of these elements exhibit appreciable solubility in Al. Moreover, the solid solubility of the RE elements, several of which form thermodynamically stable $L1_2$ trialuminides, is particularly quite low. This may be readily explained by the substantial size difference between Al and RE atoms [94].

2.3. Small diffusivity in Al

Slow diffusion kinetics are an essential requirement for retention of strength for any alloy subjected to longterm exposure at elevated temperatures. This requirement is espe-

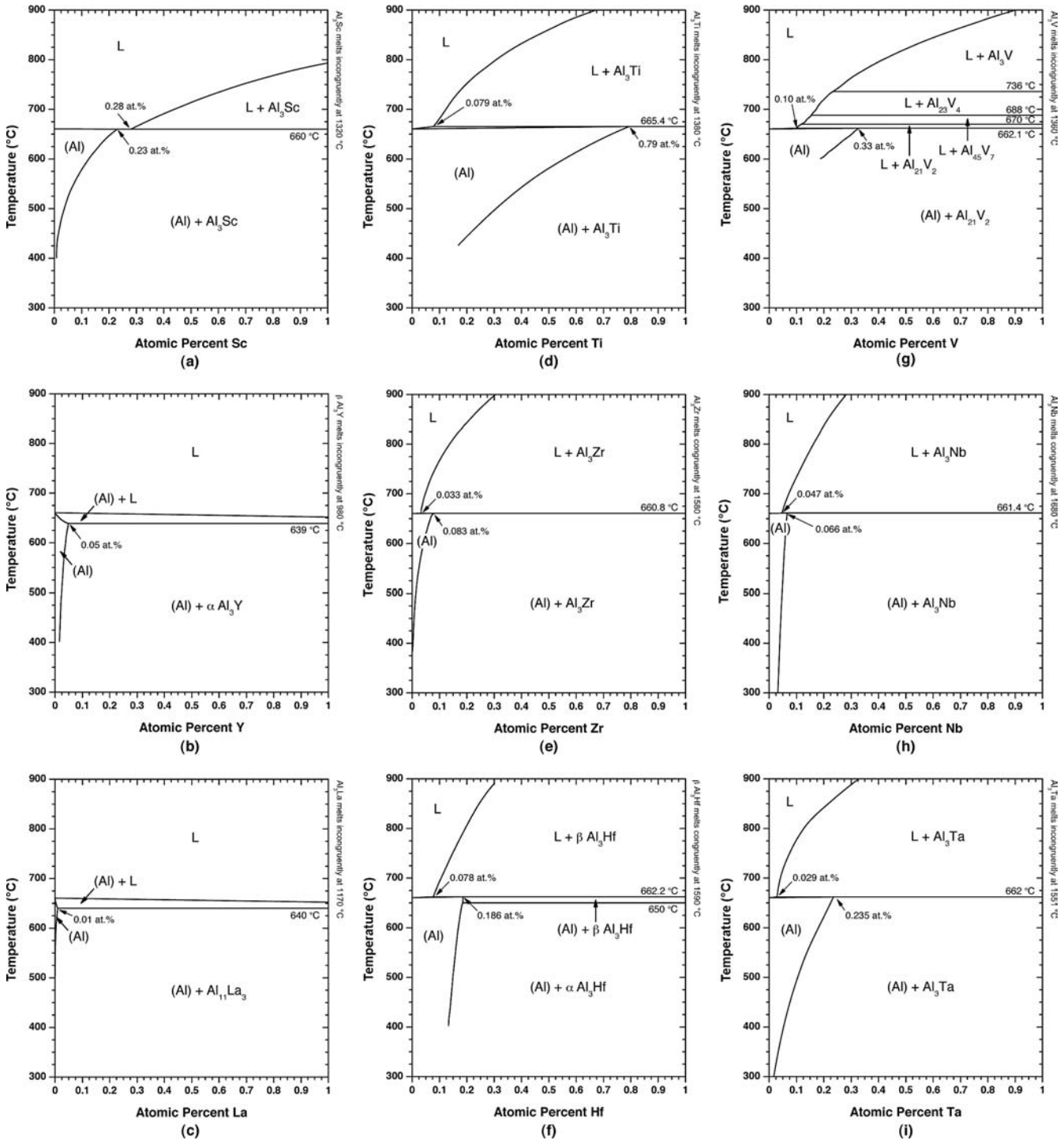

Fig. 4. Reported binary phase diagrams for dilute (< 1 at.%) additions of the Group 3, 4, and 5 transition elements alloyed with Al. References for the diagrams are: Al–Sc [42, 102]; Al–Y [42]; Al–La [42]; Al–Ti [121]; Al–Zr [122]; Al–Hf [42, 105]; Al–V [42]; Al–Nb [42, 123]; Al–Ta [42].

Table 2. Equilibrium maximum solid solubility (C_{max}) and solubility at 400 °C (C_{400}) in binary Al–M alloys that form cubic ($L1_2$) and related tetragonal ($D0_{22}$ or $D0_{23}$) Al_3M trialuminide intermetallic compounds.

Element	C_{max} (at.%)	C_{400} (at.%)	α-Al-Al_3M equilibrium	References
Group 3 transition elements				
Sc	0.23	0.01	Yes	[42, 102]
Y	0.049	0.016	Yes	[40, 42]
Group 4 transition elements				
Ti	0.79	0.13	Yes	[121]
Zr	0.083	0.0005	Yes	[122]
Hf	0.186	0.130	Yes	[42, 105]
Group 5 transition elements				
V	0.33	< 0.15	No	[42]
Nb	0.066	0.038	Yes	[42]
Ta	0.235	0.05	Yes	[42]
Lanthanide series (rare earths)				
Er	≈ 0	≈ 0	Yes	[40]
Tm	≈ 0	≈ 0	Yes	[40]
Yb[a]	0.18	< 0.1	Yes	[42]
Lu	≈ 0	≈ 0	Yes	[40]
Actinide series				
U	0.007	0.0037	No	[40, 42]
Np[b]				[40]

[a] Based on the published phase diagram in Ref. [42]. The original Refs. [125, 126] for this data, however, did not measure C_{max}. Furthermore, Ref. [40] claims there is no significant solubility of Yb in Al.
[b] No phase diagram available, although presumed to be similar to Al–U [40].

cially true for any Al-based system due to the intrinsically low volume fraction of dispersed phases and the concomitant necessity for fine precipitates with exceptional coarsening resistance (Fig. 1).

From an experimental point-of-view, it is difficult to carry out diffusion experiments in Al. Cited difficulties include the kinetic barrier for diffusion of a radioactive Al isotope through the passiviting oxide layer, the extremely low solid solubility of solutes in Al, and a strong tendency to form intermetallic compounds [128]. As a result, some of the early diffusion data for solutes in Al are unreliable. The advent of readily available radioactive isotopes after 1950, and more recent developments with ion implantation, have mitigated many of these experimental difficulties. Nevertheless, for several elements (e. g., Ti), measurements of impurity diffusion coefficients are still hampered primarily by the unavailability of suitable and inexpensive radioactive isotopes.

In light of these advances in experimental techniques, impurity diffusion in Al (especially that of the transition elements) has received renewed interest in recent years [128–132], and we review here the most reliable data, with particular emphasis on the solutes forming cubic $L1_2$ Al_3M intermetallics.

2.3.1. Trends in diffusivity among the transition elements

It is fortunate that the transition elements are anomalously slow diffusers in Al, characterized by large activation energies, large pre-exponential factors, and a wide range of variation of diffusivity values as compared with Al self-diffusion. Measured activation energies for tracer diffusion (Q) and pre-exponential factors (D_0) for all of the 3*d* transition elements and other selected 4*d*- and 5*d* transition elements are listed in Table 3. The majority of these data was obtained from two review articles by Mehrer et al. [128, 129] and Fujikawa [130], which provide the most authoritative theoretical interpretations for transition metal diffusion in Al. Data for some of the diffusing elements were also obtained from a recent review by Du et al. [130] and a somewhat older article by Grammatikakis [131]. Also, the comprehensive Landolt–Börnstein review [132] was utilized.

Data for 3*d* transition elements and of 4*sp* non-transition

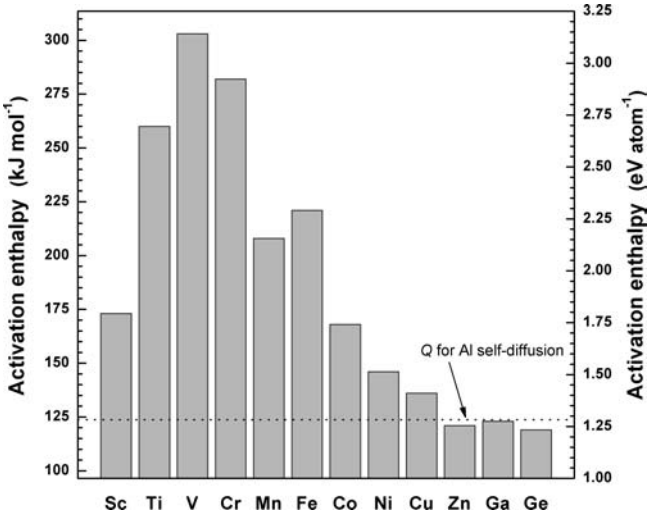

Fig. 5. Measured activation energies (Q) of 3d transition element solutes and of 4*sp* non-transition metal solutes in Al. Data for Ga and Ge are from [127].

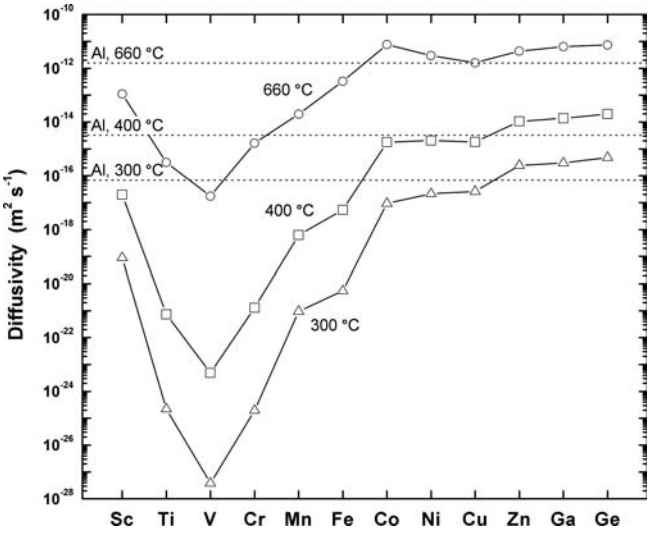

Fig. 6. Calculated diffusivities at 300, 400, and 660 °C (T_m of Al) of 3*d* transition element solutes and of 4sp non-transition metal solutes in Al. Data for Ga and Ge are from Ref. [127].

Table 3. Measured diffusion data for selected transition metal solutes in Al.

	Pre-exponential, D_0 $m^2\ s^{-1}$	Activation enthalpy, Q		D at 400 °C $m^2\ s^{-1}$	References	
		kJ mol^{-1}	eV $atom^{-1}$		Original reference	Cited in
Self-diffusion						
Al	1.37×10^{-5}	124	1.29	3.25×10^{-15}	Dais et al. [134]	[128]
Fourth period (3d) transition elements						
Sc	5.31×10^{-4}	173	1.79	1.98×10^{-17}	Fujikawa [135]	[130]
Ti	1.12×10^{-1}	260	2.69	7.39×10^{-22}	Bergner and van Chi [136]	[128, 130–132]
V	1.60	303	3.14	4.85×10^{-24}	Bergner and van Chi [136]	[128, 130–132]
Cr	10.0	282	2.92	1.29×10^{-21}	Rummel et al. [128]	[128, 130]
Mn	8.7×10^{-3}	208	2.16	6.24×10^{-19}	Rummel et al. [128]	[128, 130]
Fe	7.7×10^{-1}	221	2.29	5.41×10^{-18}	Rummel et al. [128]	[128, 130]
Co	1.93×10^{-2}	168	1.74	1.76×10^{-15}	Rummel et al. [128]	[128, 130, 131]
Ni	4.4×10^{-4}	146	1.51	2.05×10^{-15}	Erdelyi et al. [137]	[128, 130, 132, 133]
Cu	6.54×10^{-5}	136	1.41	1.54×10^{-15}	Fujikawa and Hirano [138]	[128, 130, 133]
Zn	2.59×10^{-5}	121	1.25	1.05×10^{-14}	Peterson and Rothman [139]	[128, 130, 132, 133]
Fifth period (4d) transition elements						
Zr	7.28×10^{-2}	242	2.51	1.20×10^{-20}	Marumo et al. [140]	[130, 132, 133, 141]
Mo	1.4×10^{-3}	250	2.59	5.52×10^{-23}	van Chi and Bergner [142]	[130, 132, 133]
Sixth period (5d) transition elements						
La	1.40×10^{-10}	113	1.17	2.43×10^{-19}	Murarka and Agarwala [143]	[144]
Hf	1.07×10^{-2}	241	2.50	2.11×10^{-21}	Minamino	[130]
W	1.06×10^{-3}	249	2.58	5.00×10^{-23}	van Chi and Bergner [142]	–

elements (foreign atoms from the same row of the periodic table) are depicted graphically in Figs. 5 and 6. Figure 5 shows the activation energies for tracer diffusion versus the position in the periodic table. Figure 6 shows the calculated diffusivities near the melting point of Al (660 °C) as well as two other temperatures of interest (300 and 400 °C). The 3*d* sublevel starts to fill with Sc ($Z = 21$, $[Ar]4s^2 3d^1$) and becomes filled at Zn ($Z = 30$, $[Ar]4s^2 3d^{10}$), and it is evident that valence has a strong influence on both the activation energies and the corresponding diffusivities. This dependence is most obvious in Fig. 6, where the calculated diffusivity increases with increasing number of *d* electrons from V to Co by nearly six orders of magnitude at 660 °C.

It is well known that attractive or repulsive interactions among vacancies and substitutionally dissolved solute atoms may lead to higher or lower diffusivities of solute atoms compared with the self diffusivity of the solvent atom. This relationship between the vacancy-solute binding free energy and the valence difference between solute and solvent atoms was originally discussed by Lazarus [144] and further elaborated on by LeClaire [146]. While the so-called Lazarus–LeClaire model works well for electropositive impurities in noble metals, it is known (e. g., [147, 148]) that this model is unsatisfactory for several solvents, including Al. A more accurate theoretical interpretation has been provided by Hoshino et al. [149], who studied vacancy–solute interactions in Al using *ab initio* calculations based on local-density-functional theory. These calculations indicate that while 4*sp* (and 5*sp*) solute atoms are attracted to the vacancy, the interaction for 3*d* (and 4*d*) transition elements is repulsive and exhibits a maximum near the middle of the 3*d* and 4*d* rows, which is reasonably consistent with the measured activation energies displayed in Fig. 5. Rummel et al. [129] summarize these and other theories, and provide the clearest theoretical interpretation of these interactions at present.

Alexander and Slifkin [150] noted that the row of the diffusing species – and hence atomic size – also has an influence on diffusivity. For example, the diffusivities of the Group 11 solutes increases in the sequence Cu, Ag, Au. Nevertheless, Rummel et al. [127] noted that this influence amounts to at most a factor of about 2, and is therefore minor compared to the strong valency effect. Therefore, elements of the same group may be assumed to exhibit similar diffusion kinetics in Al, as evidenced by the data for the homovalent Group 3 (Ti, Zr, Hf) and Group 6 (Cr, Mo, W) solutes in Table 3, exhibiting a factor of about 20 difference for the diffusivity at 400 °C.

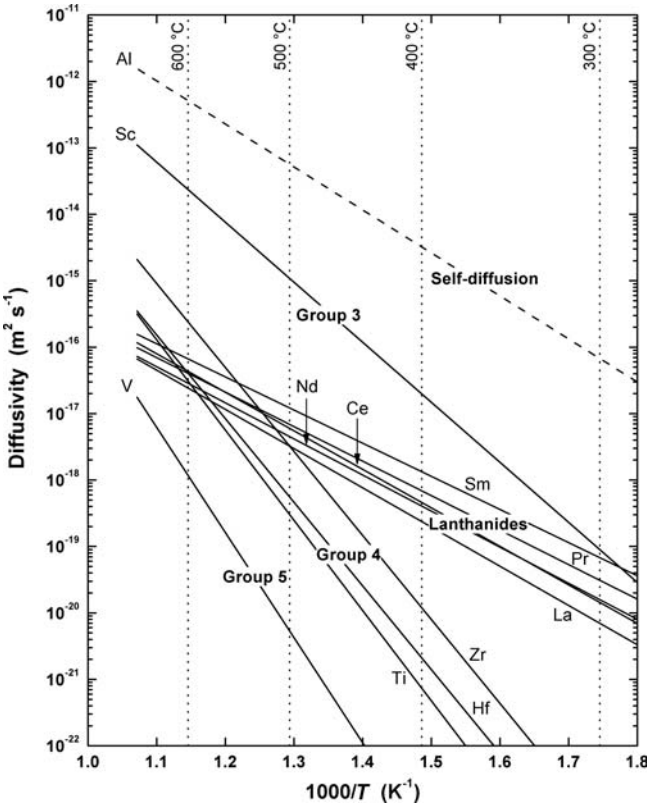

Fig. 7. Semi logarithmic plot of diffusivity in Al versus reciprocal temperature for the elements which form $L1_2$ trialuminide phases with Al. The data for Ce, Pr, Nd, and Sm are assumed to be representative of the $L1_2$-forming lanthanides (Er, Tm, Yb, and Lu).

2.3.2. Trends in diffusivity among the lanthanide elements

Reported diffusion data for the lanthanide or actinide elements in Al appear to be limited to a study by Murarka and Agarwala [143], which reports diffusion data for the early lanthanide elements (La, Ce, Pr, Nd, and Sm). These data are presented in Table 4 (Table 3 for La). As indicated, the diffusivities of the lanthanides generally lie between those of the Group 3 (Sc) and Group 4 (Ti, Zr, Hf) elements, as might be expected considering the position of the lanthanides in the periodic table. This intermediate diffusivity of the lanthanides in Al is substantiated by a decomposition study of melt spun Al–Ti, Al–Zr, and Al–Er alloys by Angers et al. [151]. The coarsening rates of the precipitated Al_3Er ($L1_2$) phases were more rapid than those for Al_3Ti ($L1_2$) or Al_3Zr ($L1_2$), most likely due to faster diffusion kinetics. The activation enthalpy for tracer diffusion is very

Table 4. Measured diffusion data for selected lanthanide solutes in Al.

	Pre-exponential, D_0 ($m^2 s^{-1}$)	Activation enthalpy, Q		D at 400 °C ($m^2 s^{-1}$)	References	
		(kJ mol^{-1})	(eV $atom^{-1}$)		Original reference	Cited in
Ce	1.9×10^{-10}	111	1.15	4.65×10^{-19}	Murarka and Agarwala [143]	[144, 152]
Pr	3.58×10^{-10}	99.4	1.03	6.94×10^{-19}	Murarka and Agarwala [143]	[144, 152]
Nd	4.8×10^{-11}	104	1.08	3.93×10^{-19}	Murarka and Agarwala [143]	[144, 152]
Sm	3.45×10^{-11}	95.5	0.99	1.33×10^{-18}	Murarka and Agarwala [143]	[144, 152]

high compared to the other elements shown in Fig. 7, and this unexpected experimental result demands that this experiment be repeated using modern analytical methods. Even more useful would be measurements of diffusivities for the other lanthanide elements.

2.3.3. Summary

The transition elements are anomalously slow diffusers in Al, with diffusivities several orders of magnitude smaller than that for Al self-diffusion. This anomalous behavior is ascribed to repulsive vacancy–solute interactions which, according to experimental evidence (Fig. 5), reaches a maximum near the Group 5 (V, Nb, Ta) column of the periodic table. The period of the diffusing species has only a moderate effect (compared to valence) and so homovalent solutes of the same group in the periodic table may be assumed to obey similar diffusion kinetics in Al. Diffusion of the lanthanide elements in Al has received comparatively little attention, but available data for the light lanthanides indicate that diffusivities are relatively small, intermediate between those of the Group 3 (Sc) and Group 4 (Ti, Zr, Hf) elements.

The diffusion behavior of elements capable of forming precipitated cubic $L1_2$ trialuminides – Al_3M formed with elements of the Group 3, Group 4, Group 5, and lanthanide series and which are in equilibrium with α-Al in Table 2 – is presented in the Arrhenius diagram of Fig. 7. The diffusion data for the early lanthanides (Ce, Pr, Nd, and Sm) is assumed to be representative of the late lanthanides (Er, Tm, Yb, Lu), which form Al_3M ($L1_2$) trialuminides.

2.4. Ability to be conventionally cast

This review is concerned with developing precipitation-strengthened Al-based alloys produced via conventional ingot metallurgy routes, which requires that any suitable system be amenable to conventional casting. We consider cast-

Table 5. Invariant reactions in binary Al–M alloys which form cubic ($L1_2$) and related tetragonal ($D0_{22}$ or $D0_{23}$) Al_3M trialuminide intermetallic compounds.

	Reaction type	Reaction temp. (°C)	Liquid solubility C_l (at.%)	Solid solubility C_{max} (at.%)	k_0	Reference
Group 3 transition elements						
Sc	Eutectic	660	0.28	0.23	0.82	[42, 102]
Y	Eutectic	639	≈ 3	0.049	≈ 0.02	[40, 42]
Group 4 transition elements						
Ti	Peritectic	665.4	0.079	0.79	10.0	[121]
Zr	Peritectic	660.8	0.033	0.083	2.52	[122]
Hf	Peritectic	662.2	0.078	0.186	2.38	[42, 105]
Group 5 transition elements						
V	Peritectic	662.1	0.10	0.33	3.3	[42]
Nb	Peritectic	661.4	0.047	0.066	1.40	[42]
Ta	Peritectic	662	0.029	0.235	8.10	[42]
Lanthanide series (rare earths)						
Er	Eutectic	655	≈ 1	≈ 0	≈ 0	[40]
Tm	Eutectic	645	1.74	≈ 0	≈ 0	[40]
Yb	Eutectic	625	3.98	0.18[a]	0.045[a]	[40, 42]
U	Eutectic	≈ 650	≈ 2	≈ 0	≈ 0	[40]
Actinide series						
U	Eutectic	646	1.7	0.007	0.004	[40, 42]
Np[b]						[40]

[a] Based on the published phase diagram in Ref. [42]. The original Refs. [126, 127] for this data, however, did not measure C_{max}. Furthermore, Ref. [40] claims there is no significant solubility of Yb in Al.
[b] No phase diagram available, although presumed to be similar to Al–U [40].

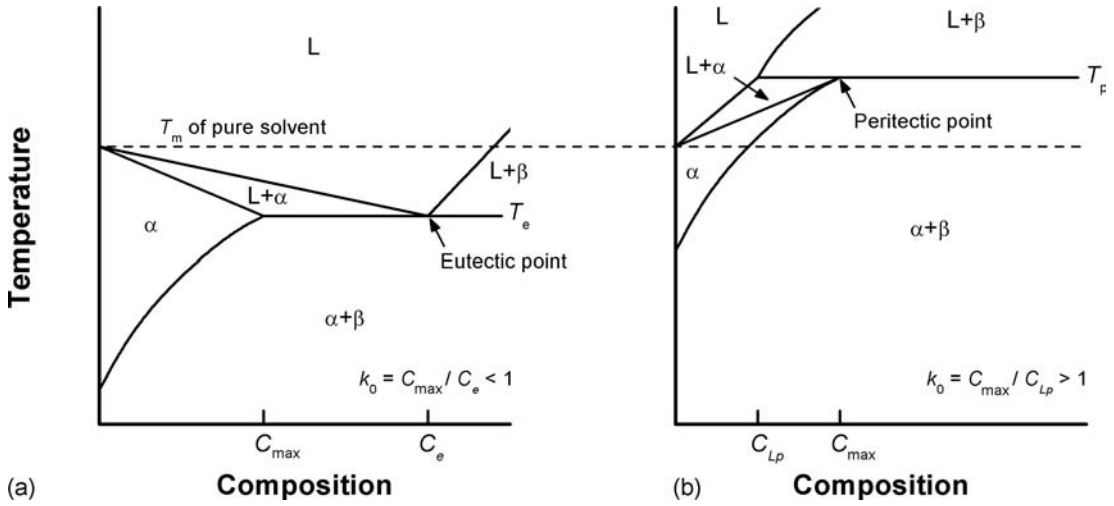

Fig. 8. Comparison between eutectic (a) and peritectic (b) reactions. In the context of the present discussion, "α" refers to α-Al and "β" refers to Al_3M.

ability only in general terms, primarily with respect to features in the reported binary phase diagrams that the various elements form with Al.

The transition elements, as well as those of the lanthanide and actinide series, form rather complex binary systems when alloyed with Al, in which one or more intermetallic phases occur [15, 17]. In these systems, eutectic phase equilibria generally exists between the liquid, the Al terminal solid solution, and the Al-rich intermetallic phase. The Al–Cu, Al–Ni, and Al–Sc systems are familiar examples. However, α-Al solid solutions are formed via the peritectic reaction between the liquid and the Al-rich intermetallic phase with the Group 4 (Ti, Zr, Hf), Group 5 (V, Nb, Ta), and Group 6 (Cr, Mo, W) transition elements. Details of the reactions are provided in Table 5 for the systems we have considered; that is, those that form cubic ($L1_2$) or related tetragonal ($D0_{22}$ or $D0_{23}$) Al_3M trialuminide phases.

2.4.1. Peritectic alloys

To appreciate the complications associated with the existence of a peritectic reaction in the phase diagram, consider Fig. 8 which compares the essential differences between eutectic and peritectic systems. These distinctions are enumerated below:

1. **The reaction itself.** Both eutectic and peritectic reactions represent invariant points (three phases in equilibrium). The eutectic reaction involves decomposition of a single phase liquid into two different solid phases ($L \rightarrow \alpha + \beta$), while the peritectic reaction is the formation of a single solid phase by the reaction of a different solid phase with the liquid ($L + \beta \rightarrow \alpha$).
2. **Solidification sequence.** In a dilute eutectic system the first solid to form is the solute-poor α solid solution, whereas for a peritectic the first solid to form can be the solute-rich β phase.
3. **Reaction temperature.** The reaction temperature is less than the melting point of pure solvent in eutectic alloys; for peritectic systems the opposite is true.
4. **Liquid-solid partition coefficient.** The equilibrium partition coefficient, k_0, for solidification of the α solid solution is less than unity in a eutectic system, while it is greater than unity in a peritectic system. This parameter dictates the solute distribution in cast alloys and therefore influences precipitation of dispersed phases during post-solidification aging.

The key difference – and limitation with regard to castability – of the Al-based peritectic systems compared to the eutectics in Table 5 relates to the solidification sequence. In an alloy of peritectic composition (that is, with composition exceeding C_{Lp}, Fig. 8b), solidified under equlibrium conditions, the first solid to form is the solute-rich primary (or properitectic) Al_3M phase. Consequently there is a strong tendency to lose a significant amount of solute to this primary phase when such peritectic alloys are conventionally cast. Moreover, as shown in Fig. 8, there is a necessary liquidus elevation with solute content in peritectic systems. Thus, in order to melt (completely) a peritectic alloy (that is, form a single-phase liquid) it is necessary to heat (and hold) the melt above this elevated temperature to dissolve completely the primary Al_3M phase. This increase in melting temperature is significant in the Al-based peritectic systems (e. g., Al–Ti, Al–Zr, Al–Nb) considering the extraordinarily high melting points of the trialuminide phases (1380 °C, 1580 °C, and 1680 °C for Al_3Ti, Al_3Zr, and Al_3Nb, respectively).

For developing a creep-resistant alloy, peritectic systems present an additional challenge due to the potent grain refinement associated with primary Al_3M precipitation in cast alloys. It is well known [123, 153–166] that minor additions of the Group 4 (Ti, Zr, Hf), Group 5 (V, Nb, Ta), and Group 6 (Cr, Mo, W) elements may be used to refine the grain structure in cast Al alloys. Though the actual mechanism is disputed [154, 157, 164], the marked grain refinement is generally attributed to the presence of primary Al_3M precipitates which act as heterogeneous nuclei during solidification of the melt. To avoid rapid diffusional creep associated with a refined grain structure it is necessary to suppress nucleation of the properitectic Al_3M phase which, for a given cooling rate, is achieved by reducing the solute content of the alloy [167–169]. Therefore, the already-limited solid solubility of most alloying elements in Al is further reduced by the necessity to avoid properitectic precipitation in the peritectic systems.

We turn now to the characteristics of the equilibrium phase diagram that are conducive to properitectic suppression. In alloys produced by RSP, the resistance of peri-

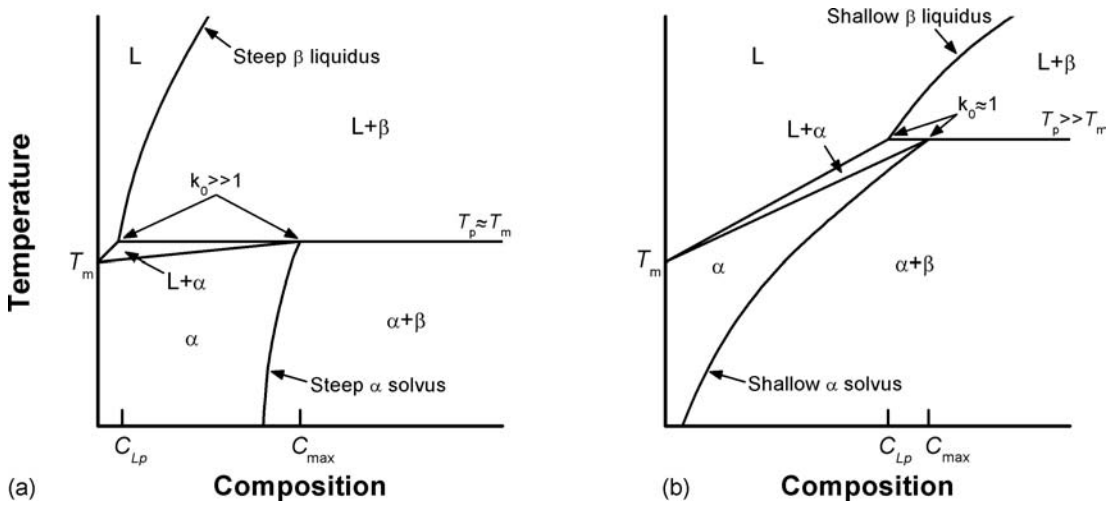

Fig. 9. Undesirable (a) and desirable (b) characteristics of peritectic systems, as they relate to the potential for development of castable precipitation-strengthened alloys.

tectic alloys to primary Al_3M formation has been shown [170, 171] to be related to the undercooling necessary to reach the metastable liquidus of the α-Al solid solution; that is, the temperature difference, at a composition of interest, between the β liquidus and extrapolated α-Al liquidus. While RSP is outside the scope of the present discussion, we may nevertheless invoke similar arguments in evaluating peritectic alloys in terms of conventional castability.

A minimum undercooling for quenching into the metastable α-Al phase field is favored in systems that have a shallow β liquidus and a steep α-Al liquidus. In the six Al-based peritectic systems of interest, the peritectic reaction temperatures are only a few degrees above the melting point of pure Al (Fig. 4, Tab. 5), and so the slopes of the α-Al liquidus curves in these systems are shallow. Therefore, the slope of the β liquidus is the primary influence determining the ease of properitectic suppression. A second approach to minimizing this undercooling (without changing the *slope* of the β liquidus) is achieved by a general increase in the solubility of β in the liquid – that is, a shift to the right of the liquidus curve.

Castability in peritectic alloys is therefore dictated primarily by the liquid solubility of solute, whereas the propensity for precipitation strengthening, as discussed previously, is determined by the solid solubility; high liquid solubilities being favored for castability and low solid solubilities required for precipitation. These criteria are conveniently expressed in terms of the equilibrium solid–liquid partition coefficient, k_0, which is the the ratio of the solute composition of the solid and liquid phases in local equilibrium during solidification [172–174][2]. Making the usual assumption that both the liquidus and solidus boundaries are straight lines, k_0 is then constant at all temperatures and may be expressed in terms of the solid and liquid compositions at the peritectic temperature: $k_0 = \frac{C_{max}}{C_{Lp}}$. All peritectic alloys exhibit partition coefficients greater than unity (Fig. 8b), and so maximum liquid solubility and minimum solid solubility is obtained in systems with partition coefficients approaching unity, that is, minimum disparity between liquid and solid solubilities.

Figure 9 shows undesirable and desirable features of hypothetical peritectic systems based on the preceding arguments. In Fig. 9a it is apparent that large undercoolings are necessary to obviate the primary β phase when casting peritectic alloys of this type. Moreover, on account of the large disparity in liquid and solid solubilities ($k_0 \gg 1$), it is difficult to achieve a significant supersaturation of solute for post-solidification aging. This reduced driving force for precipitation is exacerbated by a relatively steep α-Al solvus, that is, the solid solubility does not decrease appreciably with temperature.

The hypothetical phase diagram in Fig. 9b exhibits features favorable for conventional solidification processing. By virtue of the large liquid solubility of the β phase, a considerable amount of solute may be added before precipitating primary β during solidification. Furthermore, there is a relatively low solubility of solute at the peritectic reaction temperature ($k_0 \approx 1$), which diminishes rapidly with decreasing temperature, providing a maximum supersaturation of solute for precipitation strengthening. It is even conceivable, on account of the large liquid solubility coupled with the very low solid solubility, that nonperitectic compositions (that is, with composition less than the minimum liquid solubility of β [168]) may provide appreciable precipitation strengthening in a system resembling Fig. 9b. This is most desirable since the possibility of nucleating properitectic β, which is responsible for most of the complications of casting peritectic alloys (loss of solute during solidification and grain refinement) is eliminated.

Finally, the reaction temperature T_p in the system of Fig. 9b is much greater than that in Fig. 9a. Not only does this tend to maximize the slope of the α-Al liquidus (desirable for minimizing the undercooling necessary to suppress properitectic β) but, more importantly, such a feature is favorable in any high-temperature alloy since a high reaction temperature extends the temperature range where the reinforced two-phase (α + β) solid is thermodynamically stable. This could, in principle, extend the service temperature of the alloy beyond the melting point of pure Al.

[2] The partition coefficient k_0 is usually defined where the compositions are in wt.%. We report compositions in at.% since, assuming equal molar volumes between Al_3M and Al (reasonable considering the data in Table 1), the supersaturation (in at.%) is a direct measure of the equilibrium volume fraction of precipitated phase. Furthermore, the difference between k_0 defined by compositions in wt.% or at.% is negligible for the dilute concentrations we consider.

2.4.2. Eutectic alloys

Casting eutectic alloys (of hypoeutectic composition) is considerably less complicated than for peritectic alloys since the first solid to form is the solvent-rich α solid solution (Fig. 8a). Nevertheless, it is worthwhile commenting on a few features in the eutectic phase diagram as they relate to the potential of a given system for developing high-strength high-temperature alloys.

As in any alloy undergoing dendritic solidification, microsegregation of solute is minimized for solid-liquid partition coefficients, k_0, approaching unity. In eutectic alloys, $k_0 = \frac{C_{max}}{C_l}$ is less than unity since the α-Al liquidus has a greater solubility than the α-Al solidus, Fig. 8a. The disparity in solute solubility is what drives microsegregation, and so systems in which k_0 is near unity are especially amenable to casting, since the degree of microsegregation is small.

For high-temperature applications, a eutectic system poses a potential limitation since, by definition, the reaction temperature is less than the melting point of pure Al (Fig. 8a). In an extreme case, the eutectic reaction temperature could conceivably limit the service temperature of the alloy since its melting point is reduced. Deep Al–M binary eutectic temperatures exist for elements such as Ga and Zn, but not for those forming stable or metastable $L1_2$ trialuminides (Fig. 4, Table 5).

3. Discussion

3.1. Alloying additions with transition elements

As indicated in Table 1, transition elements that form cubic $L1_2$ trialuminides are limited to the early elements near Sc in the periodic table (Ti, Zr, Hf, V, Nb, Y), with Al_3Sc as the only thermodynamically stable $L1_2$ structure. While a metastable cubic $L1_2$ Al_3Y has been reported [44], this investigation was on highly supersaturated melt spun alloys and precipitation of Al_3Y ($L1_2$) was observed to commence during solidification. The likelihood of precipitating a similar phase in a conventionally-solidified alloy during post-solidification aging seems unlikely.

The Group 4 (Ti, Zr, Hf) and Group 5 (V, Nb, Ta) elements form metastable cubic $L1_2$ trialuminides, with the degree of metastability increasing from the former to the latter group (Section 2.1). Therefore, the Group 5 trialuminides such as Al_3Nb and Al_3Ta are poor candidates for cubic $L1_2$ modification. Indeed, as indicated in Table 1, the existence Al_3Ta ($L1_2$) is unknown to the authors. This is unfortunate, since both the Al–Nb and Al–Ta peritectic systems (Figs. 4h and 4i, respectively) exhibit favorable characteristics (small k_0 and limited solid solubility, C_{400}) and, considering they are also Group 5 elements, should also be very slow diffusers in Al (Fig. 7). Furthermore, unlike the Group 4 (Ti, Zr, Hf) elements, reports of precipitation during aging of Al–Nb and Al–Ta alloys are unknown to the authors. Among the transition elements, therefore, only Sc and the neighboring Group 4 (Ti, Zr, Hf) elements seem to offer the most potential for producing a precipitated dispersion of $L1_2$ precipitates formed during solid-state aging.

3.1.1. Stable $L1_2$ Sc trialuminide precipitates

Aside from being the only transition element forming a thermodynamically stable cubic $L1_2$ trialuminide, the Al–Sc system exhibits other unique features that make it attractive for developing conventionally-cast precipitation-strengthened alloys. As displayed in Fig. 4a and Table 5, the eutectic Al–Sc system features an exceptionally high reaction temperature (660 °C, within 1 K of the melting point of pure Al), with a relatively high solid solubility (0.23 at.% Sc) and comparatively low liquid solubility (0.28 at.% Sc) at the reaction temperature. This similarity in solid and liquid solubilities leads to an equilibrium partition coefficient, k_0, very near unity ($k_0 = 0.82$, Table 5) which minimizes segregation during solidification and makes this system especially amenable to conventional casting. The extremely high eutectic temperature does not limit the service temperature of Al–Sc alloys for high-temperature applications. In fact, the liquid and solid eutectic solubilities are so close and the reaction temperature so high that the first published phase diagrams for Al–Sc indicated a terminal peritectic reaction like the neighboring Al–Ti, Al–Zr, and Al–Hf systems [43].

The maximum solid solubility of Sc in Al is relatively large, exceeded for the elements in Table 2 only by Ti and V (and similar to Ta), and it diminishes significantly with decreasing temperature ($C_{400} = 0.01$ at.% Sc, Fig. 4a and Table 2), thus maximizing the volume fraction of Al_3Sc achievable during post-solidification aging. Of the systems in Table 2, only Al–Ti and Al–Ta exhibit a comparably high decrease in solid solubility with temperature. This fortuitous confluence of desirable characteristics – a stable $L1_2$ trialuminide, a solvus boundary conducive to precipitation strengthening, eutectic phase equilibria favoring conventional solidification, and a very high eutectic temperature – makes the Al–Sc system particularly well-suited for developing castable, precipitation-strengthened alloys. Additions of Sc, forming coherent nanoscale Al_3Sc ($L1_2$) precipitates, provide the highest increment of strengthening (at room temperature) per atomic percent of any alloying element when added to Al [175]. In addition to the marked precipitation-hardening response, these precipitates are also very effective at inhibiting recrystallization and maintaining a fine uniform microstructure in wrought Al alloys [43].

The potent strengthening from precipitated Al_3Sc ($L1_2$), the high eutectic temperature, and the relatively low diffusivity of Sc in Al (Fig. 7) indicate that Al-Sc alloys possess significant potential for developing conventionally-solidified creep-resistant Al-based alloys. Indeed, recent studies by Dunand, Seidman, and colleagues have shown conventionally-solidified Al–Sc alloys exhibiting remarkably high coarsening and creep resistance at 300 °C [176, 177], which may be improved with ternary additions of Mg [178–180], Zr [114–116], and Ti [117]. The latter two elements, together with many other candidates with diffusivities below that of Sc [119], segregate to the Al_3Sc phase without changing its $L1_2$ structure. These Sc substitutions also reduce the relatively high cost of Sc additions.

3.1.2. Metastable $L1_2$ trialuminides of the Group 4 transition elements

The Group 4 transition elements (Ti, Zr, Hf) are extremely slow diffusers in Al (Fig. 7), and therefore offer potentially

significant improvements in thermal stability compared to Al–Sc alloys. While the $L1_2$ trialuminides formed from the Group 4 elements are metastable, these are slow to transform to their respective equilibrium tetragonal structures (Section 2.1.1) and therefore seem promising as thermally stable dispersed phases in high-temperature Al-based alloys. The Group 4 elements, however, form peritectics with Al which, as discussed in Section 2.4, introduces significant complications to produce alloys by conventional ingot metallurgy routes.

The Al–Ti system (Fig. 4d) seems especially attractive due to the very sluggish diffusion kinetics of Ti in Al (Fig. 7). Moreover, of all the systems in Table 2, Ti has the highest maximum solid solubility in Al (0.79 at.% Ti), suggesting that relatively high volume fractions of precipitated Al_3Ti may be obtained. The Al–Ti system has, however, a comparatively limited liquid solubility (k_0 = 10.0, Table 5). Hence, for alloy compositions approaching the maximum solubility there will be a strong tendency for primary Al_3Ti precipitation during solidification and so appreciable Ti concentrations are unlikely to remain in solid solution after conventional solidification. Moreover, the solid solubility of Ti is still rather large at appropriate aging temperatures (C_{400} = 0.13 at.% Ti), limiting both the chemical driving force for nucleation and the volume fraction of the dispersed phase (if formed). As reviewed by the authors [181], virtually all precipitation studies for the Al–Ti system have investigated alloys prepared by nonequilibrium means: RSP and MA, techniques which circumvent the difficulties encountered during conventional solidification of Al–Ti alloys.

In the Al–Hf system (Fig. 4f) there is a relatively small disparity between the liquid and solid solubilities at the peritectic temperature (k_0 = 2.38, Table 5), implying that alloys with compositions corresponding to the maximum solubility (0.186 at.% Hf, Table 2) may be obtained with conventional casting techniques. This solid solubility, however, diminishes only slightly with decreasing temperature (C_{400} = 0.130 at.% Hf, Fig. 4f and Table 2) which limits the potential for precipitation strengthening. Indeed, in all of the precipitation studies on Al–Hf alloys cited previously [84–92], the alloys were generally highly supersaturated and produced by relatively rapid (nonequilibrium) chill casting methods. Ryum [84], for example, investigated the decomposition of relatively supersaturated 0.27 at.% Hf solid solutions produced by chill casting. Although the cooling rate was not reported in [84], it is reasonable to believe it was about $3 \cdot 10^3$ °C s^{-1}, which was the solidification rate reported by Hori et al. [85, 86, 90, 91] on investigations of chill cast alloys containing up to 0.79 at.% Hf. It was reported [85–87] that the solid solubility of Hf in Al could be extended to approximately 0.5 at.% Hf at this cooling rate, and such high values of supersaturations, well in excess of the maximum solid solubility, were required to effect continuous precipitation of Al_3Hf ($L1_2$) [87], with a pronounced precipitation hardening response in alloys aged at 350 to 450 °C [85, 86]. Other studies investigated even more supersaturated alloys (up to 1.0 at.% Hf) obtained by rapid solidification at a rate of approximately 10^7 K s^{-1} [87, 89, 92].

Unlike Ti and Hf, Zr exhibits negligible solubility in Al at temperatures of interest for post-solidification aging (C_{400} < 0.001 at.% Zr, Fig. 4e and Table 2). Consequently, even very dilute alloying additions may produce an appreciable precipitation hardening response as shown by Hori et al. [182, 183], who reported precipitation hardening in alloys containing 0.07 at.% Zr aged at 350 to 450 °C. Ichikawa and Ohashi [184] similarly observed a significant age hardening response when dilute chill cast alloys, containing as little as 0.12 at.% Zr, were aged at 300 to 500 °C. Furthermore, Nes [78] has reported precipitation of Al_3Zr ($L1_2$) in very dilute (hypoperitectic, 0.05 at.% Zr) alloys.

Moreover, the role of dilute additions of Zr to commercial wrought alloys as recrystallization inhibitors is well known [77, 185–188], where fine (20 to 30 nm) dispersions of coherent Al_3Zr ($L1_2$) precipitates are used to pin grain and subgrain boundaries during annealing. The Zr concentration required to inhibit recrystallization in conventionally cast commercial alloys is very low, typically 0.03 to 0.06 at.% Zr [188].

3.2. Alloying additions with lanthanide elements

There would seem to exist significant potential for the use of late rare earth elements (Er, Tm, Yb, Lu) in Al, as they form thermodynamically stable $L1_2$ trialuminides (Fig. 2), are likely slower diffusers than Sc (Fig. 7), and, unlike the Group 4 elements, exhibit the preferred eutectic phase equilibrium (Table 5), which is favorable for conventional ingot metallurgy processing. Indeed, a number of Al–RE systems – Al–La [99, 189–191], Al–Ce [192, 193], Al–Nd [192, 194, 195], Al–Gd [97, 98, 195, 196], Al–Sm [98], and Al–Er [98, 151, 189, 195, 197–199], in particular – have received considerable attention for development into dispersion-strengthened alloys for elevated temperature applications. All of these studies, however, investigated highly-supersaturated (sometimes hypereutectic) alloys prepared by RSP. The attraction to the RE elements stems from their generally high solubility in the liquid state, very limited solid solubility, and low solid state diffusivity in Al. The high liquid solubility is conducive to solid solubility extension by RSP, while the very limited solid solubility and small diffusivity retards volume diffusion-controlled coarsening of the dispersed intermetallic phases during thermal exposure.

As in the Al–Fe-based alloys described previously, the strengthening dispersions in these alloys form during solidification, either as lamellar eutectic constituents, as a primary phase in hypereutectic alloys, or are precipitated in the solid state on cooling from solidification. The microstructures in these rapidly-solidified alloys, as monitored by microhardness, are generally stable beyond 300 °C [97, 189, 190, 192–194, 196, 198, 199], as might be anticipated due to the low diffusivity and solid solubility of the RE elements in Al.

Since the strengthening dispersions form on solidification, precipitation hardening during post solidification aging is generally not observed in these alloys. This lack of hardening is a consequence of the very limited equilibrium solubility of the RE elements in Al (Table 2), which assures almost complete precipitation of solute on cooling. Even in highly supersaturated Al–La (0.8 at.% La [189, 190]) and Al–Er (0.7 at.% Er [189, 199]) alloys produced by RSP, the amount of La and Er retained in solid solution was negligible as indicated by lattice parameter measurements using X-ray diffraction (XRD) of the as-solidified α-Al solid solution.

Solid-state precipitation of Al_3Er ($L1_2$) has, however, been reported by Angers et al. [151] in extremely supersaturated (hypereutectic) rapidly-solidified Al–Er alloys containing 6.25 at.% Er. Furthermore, a weak indication of additional precipitation hardening (beyond the strengthening provided by the as-solidifed dispersions) was shown in other studies on Al–Er alloys [198], as well as Al–Gd alloys [97,196], but the origin of this hardness increase was not reported.

More support for Al–Er as a promising system capable of precipitation strengthening may be provided by Nie et al. [200–202], who indicated that coherent nanoscale Al_3Er ($L1_2$) dispersions can be potent recrystallization inhibitors in Al alloys, comparable in effect to the more commonly-used Al_3Zr and Al_3Sc phases in commercial alloys. Although their experimental techniques were not explicit about this point, micrographs indicate that coherent Al_3Er precipitates were not precipitated during aging but rather formed during cooling after solidification, similar to what Foley et al. [44] reported for metastable Al_3Y ($L1_2$) precipitation described previously.

While the Al–RE systems show considerable promise for development by RSP, their conduciveness to conventional solidification is limited. Indeed, the very properties which makes the Al–RE systems attractive for RSP, namely a very high liquid solubility and low solid solubility (in other words $k_0 \ll 1$), limits their potential when these alloys are produced by conventional casting techniques. Because of the very limited solid solubility, a supersaturation of solute is impossible to achieve under moderate cooling rates since there will be a strong driving force for precipitation during cooling, as shown in studies on Al–Er [200, 201] and Al–Y [44]. A partition coefficient deviating far from unity also predicts that these alloys will be prone to significant solute segregation during solidification, as substantiated by Ruder and Eliezer [190, 199] comparing the microstructures of Al–La and Al–Er solidified conventionally and with RSP. Moreover, due to the very limited maximum solid solubility of the RE elements in Al (Table 2), post-solidification homogenization is not possible.

3.3. Summary

It is an unfortunate coincidence that the slowest diffusers in Al – that is, the Groups 4 to 6 transition elements – are also the only elements in the periodic table forming terminal peritectics with Al (all other alloying additions exhibit eutectic or monotectic phase equilibria) [15]. The existence of a peritectic reaction in the phase diagram reduces significantly the conduciveness of these systems to conventional casting. It is equally unfortunate that all of the late lanthanide elements, with the possible exception of Yb (see notes in Tabs. 2 and 5), exhibit negligible solid solubility in Al. This severely limits the potential for precipitation strengthening since virtually all available solute is precipitated out of solid solution during post-solidification cooling.

The Group 3 element, Sc, exhibits a unique eutectic phase equilibrium with Al which makes it particularly conducive to developing conventionally-solidified precipitation strengthened alloys. Moreover, Al_3Sc is a thermodynamically stable $L1_2$ trialuminide which exists in two-phase equilibrium with Al to the high eutectic temperature of 660 °C. Unfortunately, the very high cost of Sc limits its applications. Moreover, compared to the other transition elements, Sc is only a moderately slow diffuser in Al (Fig. 7).

Of the slower-diffusing peritectic-forming elements which form $L1_2$ trialuminides (Groups 4 and 5), the Group 4 are strongly favored since the $L1_2$ structure in these systems is only slightly metastable. Of the Group 4 elements, only Zr exhibits negligible solubility at suitable aging temperatures (Fig. 4), both maximizing the volume fraction of the precipitated Al_3Zr phase as well as improving its resistance to coarsening.

4. Conclusions

This review has summarized basic criteria required for a conventionally-solidified precipitation-strengthened Al-based alloy for high-temperature applications:

(i) Solid-state precipitation upon aging of coherent trialuminide Al_3M with the $L1_2$ crystal structure, to achieve high strengthening and low coarsening;
(ii) Shallow α-Al solvus curve, to maximize the volume fraction of precipitated Al_3M (and thus increase strengthening); and the concomitant low solid solubility at the aging temperature to minimize coarsening;
(iii) Low diffusivity of M in Al, to minimize Al_3M coarsening and the associated loss of strength;
(iv) Solid-liquid partition coefficient (k_0) near unity, to minimize segregation and accommodate conventional solidification. For peritectic systems, a shallow Al_3M liquidus boundary is desirable for minimizing the casting temperature and suppressing Al_3M primary precipitation during solidification.

Criterion (i) narrows the potential candidates to only eight elements, all situated near Sc in the periodic table: the first Group 3 element (Sc), the three Group 4 elements (Ti, Zr, Hf) and the four heaviest rare-earth elements (Er, Tm, Yb, Lu). Among these elements, Sc and Zr stand out for the following reasons:

- The Al–Sc system exhibits a unique combination of a shallow solvus curve conducive to precipitation strengthening, an eutectic phase equilibrium favoring conventional solidification, and thermodynamically stable Al_3Sc with the $L1_2$ structure. Sc is, however, the fastest diffuser in Al and the priciest of the above eight elements.
- The Al–Zr system is characterized by one of the lowest diffusion rates and lattice parameter mismatch between Al_3M and Al, as well as price among the eight candidates. The $L1_2$ structure of Al_3Zr, however, is metastable. Furthermore, the Al–Zr system is peritectic which limits the concentration of Zr retained in solid solution after conventional solidification, ultimately limiting the strength attainable by precipitation strengthening. Unlike the other Group 4 systems (Al–Ti and Al–Hf), the solid solubility of Zr in Al is negligible and so precipitation strengthening can be obtained in conventionally cast alloys. The steep α-Al solvus, however, limits the possibility of post-solidification homogenization.

This research is supported by the United States Department of Energy, Basic Sciences Division, under contract DE-FG02-02ER45997. We thank Profs. M. E. Fine and M. Asta (Northwestern University) and Dr. J. L. Murray (Alcoa) for numerous useful discussions. We are also pleased to acknowledge R. A. Karnesky and M. E. van Dalen (Northwestern University) for assistance with some of the data for the rare earth elements.

References

[1] M.E. Fine: Metall. Trans. A 6 (1975) 625.
[2] C.M. Adam, in: B.H. Kear, B.C. Giessen, M. Cohen (Eds.), Rapidly Solidified Amorphous and Crystalline Alloys. Elsevier, Boston (1982) 411.
[3] W.M. Griffith, J. Sanders, G.J. Hildeman, in: M.J. Koczak, G.J. Hildeman (Eds.), High-Strength Powder Metallurgy Aluminum Alloys. Metallurgical Society of AIME, Warrandale (1982) 209.
[4] Y.W. Kim, W.M. Griffith (Eds.): Dispersion Strengthened Aluminum Alloys. TMS, Warrendale (1988).
[5] D.J. Skinner, K. Okazaki: Scripta Metall 18 (1984) 905.
[6] D.J. Skinner, R.L. Bye, D. Raybould, A.M. Brown: Scripta Metall 20 (1986) 867.
[7] D.J. Skinner, in: Y.W. Kim, W.M. Griffith (Eds.), Dispersion Strengthened Aluminum Alloys. TMS (1988) 181.
[8] D.J. Skinner, K. Okazaki, C.M. Adam, in: M.E. Fine, E.A. Starke (Eds.), Rapidly Solidified Powder Aluminum Alloys, ASTM STP 890. ASTM, Philadelphia (1986) 211.
[9] G. Thursfield, M.J. Stowell: J. Mater. Sci. 9 (1974) 1644.
[10] Y.W. Kim, W.M. Griffith, in: M.E. Fine, E.A. Starke (Eds.), Rapidly Solidified Powder Aluminum Alloys, ASTM STP 890. ASTM, Philadelphia (1986) 485.
[11] E. Hornbogen, E.A. Starke: Acta Metall. Mater. 41 (1993) 1.
[12] A.W. Zhu, B.M. Gable, G.J. Shiflet, E.A. Starke: Adv. Eng. Mater. 4 (2002) 839.
[13] A.W. Zhu, B.M. Gable, G.J. Shiflet, E.A. Starke, in: Aluminum Alloys 2002: Their Physical and Mechanical Properties Pts. 1–3, Vol. 396-4 of Materials Science Forum (2002) 21.
[14] E. Sahin, H. Jones, in: B. Cantor (Ed.), Rapidly Quenched Metals II. The Metals Society, London (1978) 138.
[15] J.E. Hatch: Aluminum, Properties and Physical Metallurgy. American Society for Metals, Metals Park (1984).
[16] H. Jones, in: Y.W. Kim, W.M. Griffith (Eds.), Dispersion Strengthened Aluminum Alloys. TMS (1988) 57.
[17] F.H. Froes, Y.W. Kim, S. Krishnamurthy: Mater Sci Eng A 117 (1989) 19.
[18] E. Orowan, in: Symposium on Internal Stresses in Metals and Alloys. Institute of Metals, London (1948) 451.
[19] R.F. Decker: Metall. Trans. 4 (1973) 2495.
[20] A.J. Ardell: Metall Trans A 16 (1985) 2131.
[21] J.W. Martin: Micromechanisms in Particle Hardened Alloys. Cambridge University Press (1980).
[22] E. Nembach: Particle Strengthening of Metals and Alloys. John Wiley & Sons, New York (1997).
[23] A. Ardell, in: J.H. Westbrook, R.L. Fleischer (Eds.), Intermetallic Compounds: Principles and Practice, Vol. 2. John Wiley & Sons (1994) 257.
[24] J.W Martin: Precipitation Hardening. Second ed., Butterworth-Heinemann, Boston (1998).
[25] P. Hirsch, F. Humphreys, in: A.S. Argon (Ed.), Physics of Strength and Plasticity. MIT Press, Cambridge, MA (1969) 189.
[26] M.A. Meyers, K.K. Chawla: Mechanical Metallurgy: Principles and Applications. Prentice-Hall, New Jersey (1984).
[27] H.J. Frost, M.F. Ashby: Deformation-Mechanism Maps: The Plasticity and Creep of Metals and Ceramics. Pergamon Press, New York (1982).
[28] T.M. Pollock, A.S. Argon: Acta Metall. Mater. 40 (1992) 1.
[29] J.H. Westbrook, in: F.R.N. Nabarro, M.S. Duesberry (Eds.), Vol. 10: $L1_2$ Ordered Alloys, Dislocations in Solids. Elsevier, Amsterdam (1996) 1.
[30] J. Rösler, E. Arzt: Acta Metall. 36 (1988) 1043.
[31] E. Arzt: Res. Mech. 31 (1991) 399.
[32] E. Arzt, in: S. Ochiai (Ed.), Mechanical Properties of Metallic Composites. Marcel Dekker, Inc., New York (1994) 205.
[33] E.A. Marquis, D.C. Dunand: Scripta Mater 47 (2002) 503.
[34] I.M. Lifshitz, V.V. Slyozov: J. Phys. Chem. Solids 19 (1961) 35.
[35] C. Wagner: Z. Elektrochemie 65 (1961) 581.
[36] H.A. Calderon, P.W. Voorhees, J.L. Murray, G. Kostorz: Acta Metall. Mater. 42 (1994) 991.
[37] L.M. Angers, Y.C. Chen, M.E. Fine, J.R. Weertman, M.S. Zedalis, in: E.A. Starke, T.H. Sanders (Eds.), Aluminum Alloys: Their Physical and Mechanical Properties, Vol. 1. EMAS, Warley (1986) 321.
[38] M.E. Fine, in: Y.W. Kim, W.M. Griffith (Eds.), Dispersion Strengthened Aluminum Alloys. TMS (1988) 103.
[39] S.K. Das, in: J.H. Westbrook, R.L. Fleischer (Eds.), Intermetallic Compounds: Principles and Practice, Vol. 2. John Wiley & Sons (1994) 175.
[40] T.B. Massalski (Ed.): Binary Alloy Phase Diagrams, Vol. 1., 2nd ed. ASM International, Materials Park (1990).
[41] H. Okamoto: Phase Diagrams for Binary Alloys. ASM International, Materials Park (2000).
[42] H. Okamoto: Phase Diagrams of Dilute Binary Alloys. ASM International, Materials Park (2002).
[43] J. Royset, N. Ryum: Int. Mater. Rev. 50 (2005) 19.
[44] J.C. Foley J.H. Perepezko, D.J. Skinner: Mater. Sci. Eng. A 179 (1994) 205.
[45] M. Yamaguchi, H. Inui, in: J.H. Westbrook, R.L. Fleischer (Eds.), Intermetallic Compounds: Principles and Practice, Vol. 2. John Wiley & Sons (1994), 147.
[46] R.L. Fleischer, D.M. Dimiduk, H.A. Lipsitt: Annual Review of Materials Science 19 (1989) 231.
[47] K.S. Kumar: Int. Mater. Rev. 35 (1990) 293.
[48] E.P. George, D.P. Pope, C.L. Fu, J.H. Schneibel: ISIJ Int. 31 (1991) 1063.
[49] K.S. Kumar, in: N.S. Stoloff, V.K. Sikka (Eds.), Physical Metallurgy and Processing of Intermetallic Compounds. Chapman and Hall (1996) 392.
[50] V.A. Raman, K. Schubert: Z. Metallkd. 56 (1965) 40.
[51] S. Mazdiyasni, D.B. Miracle, D.M. Dimiduk, M.G. Mendiratta, P.R. Subramanian: Scripta Metall. 23 (1989) 327.
[52] A.E. Carlsson, P.J. Meschter: J. Mater. Res. 5 (1990) 2813.
[53] J.P. Nic, S. Zhang, D.E. Mikkola: Scripta Metall. Mater. 24 (1990) 1099.
[54] S. Zhang, J.P. Nic, D.E. Mikkola: Scripta Metall. Mater. 24 (1990) 57.
[55] D.E. Mikkola, J.P. Nic, S. Zhang, W.W. Milligan: ISIJ Int. 31 (1991) 1076.
[56] Y. Ma, T. Arnesen, J. Gjonnes, J. Tafto: J. Mater. Res. 7 (1992) 1722.
[57] C. Amador, J.J. Hoyt, B.C. Chakoumakos, D. Defontaine: Phys. Rev. Lett. 74 (1995) 4955.
[58] Y. Nakayama, H. Mabuchi: Intermetallics 1 (1993) 41.
[59] M. Takeda, T. Kikuchi, S. Makihara: J. Mater. Sci. Lett. 18 (1999) 631.
[60] S.S. Nayak, B.S. Murty: Mater. Sci. Eng. A 367 (2004) 218.
[61] P.B. Desch, R.B. Schwarz, P. Nash: J. Less-Common Metals 168 (1991) 69.
[62] K.I. Moon, K.Y. Chang, K.S. Lee: J. Alloys Compounds 312 (2000) 273.
[63] K.I. Moon, S.C. Kim, K.S. Lee: Intermetallics 10 (2002) 185.
[64] K.I. Moon, S.H. Lee, J.K. Seon: Intermetallics 10 (2002) 793.
[65] A.E. Carlsson, P.J. Meschter: J. Mater. Res. 4 (1989) 1060.
[66] J.H. Xu, A.J. Freeman: Phys. Rev. B 40 (1989) 11927.
[67] J.H. Xu, A.J. Freeman: J. Mater. Res. 6 (1991) 1188.
[68] P.R. Subramanian, J.P. Simmons, M.G. Mendiratta, D.M. Dimiduk, in: C.T. Liu, A.I. Taub, N.S. Stoloff, C.C. Koch (Eds.), High-Temperature Ordered Intermetallic Alloys III, Vol. 133. MRS, Pittsburgh (1989) 51.
[69] T. Ohashi, R. Ichikawa: J. Japan. Inst. Light. Metals 27 (1977) 105.
[70] S. Hori, H. Tai, Y. Narita, in: S. Steeb, H. Warlimont (Eds.), Rapidly Quenched Metals, Proceedings of the Fifth International Conference on Rapidly Quenched Metals. Würzburg, Elsevier Science Publishers (1985) 911.
[71] A. Majumdar, R.H. Mair, B.C. Muddle, in: M. Tenhover, W.L. Johnson, L.E. Tanner (Eds.), Science and Technology of Rapidly Quenched Alloys, Vol. 80. Materials Research Society, Boston (1987) 253.
[72] J.F. Nie, A. Majumdar, B.C. Muddle: Mater. Sci. Eng. A 179 (1994) 619.
[73] J.F. Nie, B.C. Muddle: Mater. Sci. Eng. A 221 (1996) 11.
[74] J.F. Nie, B.C. Muddle: Mater. Sci. Eng. A 221 (1996) 22.
[75] O. Izumi, D. Oelschlägel: Scripta Metall. 3 (1969) 619.
[76] O. Izumi, D. Oelschlägel: Z. Metallkd. 60 (1969) 845.
[77] N. Ryum: Acta Metall. 17 (1969) 269.
[78] E. Nes: Acta Metall. 20 (1972) 499.
[79] S. Hori, T. Kitagawa, T. Masutani, A. Takehara: J. Japan. Inst. Light. Metals 27 (1977) 129.
[80] S. Hori, T. Kondo, S. Ikeno: J. Japan. Inst. Light. Metals 28 (1978) 79.
[81] W. Dahl, W. Gruhl, W.G. Burchard, G. Ibe, C. Dumitrescu: Z. Metallkd. 68 (1977) 188.

[82] Z.A. Chaudhury, C. Suryanarayana: Metallography 17 (1984) 231.
[83] M.S. Zedalis, M.E. Fine: Metall. Trans. A 17 (1986) 2187.
[84] N. Ryum: J. Mater. Sci. 10 (1975) 2075.
[85] S. Hori, N. Furushiro, W. Fujitani: Aluminium 57 (1981) 556.
[86] S. Hori, N. Furushiro, W. Fujitani: J. Japan Inst. Light. Metals 30 (1980) 617.
[87] S. Hori, N. Furushiro, in: T. Masumoto, K. Suzuki (Eds.), Proc. 4th Int. Conf on Rapidly Quenched Metals, Vol. 2. The Japan Institute of Metals, Sendai, Japan (1981) 1525.
[88] S. Hori, N. Furushiro, W. Fujitani: J. Japan Inst. Light Metals 31 (1981) 649.
[89] S. Hori, Y. Unigame, N. Furushiro, H. Tai: J. Japan Inst. Light Metals 32 (1982) 408.
[90] N. Furushiro, S. Hori, in: S. Steeb, H. Warlimont (Eds.), Rapidly Quenched Metals, Proceedings of the Fifth International Conference on Rapidly Quenched Metals, Würzburg, Elsevier Science Publishers (1985) 907.
[91] N. Furushiro, S. Hori: Acta Metall. 33 (1985) 867.
[92] S.K. Pandey C. Suryanarayana: Mater. Sci. Eng. A 111 (1989) 181.
[93] S. Srinivasan, P.B. Desch, R.B. Schwarz: Scripta Metall Mater 25 (1991) 2513.
[94] K.H.J. Buschow, J.H. Vanvucht: Philips Research Reports 22 (1967) 233.
[95] J.F. Cannon, H.T. Hall: J. Less-Common Metals 40 (1975) 313.
[96] M.X. Quan, P. Haldar, J. Werth, B.C. Giessen, in: B.C. Giessen, D.E. Polk, A.I. Taub (Eds.), Rapidly Solidified Alloys and Their Mechanical and Magnetic Properties, Vol. 58. MRS, Pittsburgh (1986) 299.
[97] S.J. Savage, D. Eliezer, F.H. Froes: Metall. Trans. A 18 (1987) 1533.
[98] S.J. Savage, F.H. Froes, D. Eliezer, in: P.W. Lee, R.S. Carbonara (Eds.), Rapidly Solidified Materials. ASM, Metals Park (1986) 351.
[99] B. Dill, Y. Li, M. Al-Khafaji, W.M. Rainforth, R.A. Buckley: J. Mater. Sci. 29 (1994) 3913.
[100] M. Al-Khafaji, Y. Li, W.M. Rainforth, H. Jones: Phil. Mag. B 70 (1994) 1129.
[101] A. Meyer: J. Less-Common Metals 20 (1970) 353.
[102] J.L. Murray: J. Phase Equil. 19 (1998) 380.
[103] E.A. Brandes, G.B. Brook (Eds.): Smithells Metals Reference Book. 7th ed. Butterworth-Heinemann, Oxford (1992).
[104] K.S. Vecchio, D.B. Williams: Acta Metall. 35 (1987) 2959.
[105] J.L. Murray, A.J. McAlister, D.J. Kahan: J. Phase Equil. 19 (1998) 376.
[106] P. Villars, A. Prince, H. Okamoto: Handbook of Ternary Alloy Phase Diagrams, Vol. 1. ASM International, Materials Park (1995).
[107] O.I. Zalutskaya, V.R. Ryabov, I.I. Zalutsky: Dopovidi Akademii Nauk Ukrainskoi RSR Seriya A-Fiziko-Matematichni Ta Technichni Nauki (1969) 255.
[108] G. Petzow, G. Effenberg (Eds.): Ternary Alloys: A Comprehensive Compendium of Evaluated Constitutional Data and Phase Diagrams, Vol. 5. VCH, Weinheim (1992).
[109] S. Tsunekawa, M.E. Fine: Scripta Metall 16 (1982) 391.
[110] M. Zedalis, M.E. Fine: Scripta Metall 17 (1983) 1247.
[111] R.E. Lewis, D.D. Crooks, Y.C. Chen, M.E. Fine, J.R. Weertman, in: B. Wilshire, R.W. Evans (Eds.), Proc. 3rd Int. Conf on Creep and Fracture of Engineering Materials and Structures. The Institute of Metals, London (1987) 331.
[112] Y.C. Chen, M.E. Fine, J.R. Weertman, R.E. Lewis: Scripta Metall. 21 (1987) 1003.
[113] Y.C. Chen, M.E. Fine, J.R. Weertman: Acta Metall. Mater. 38 (1990) 771.
[114] C.B. Fuller, D.N. Seidman, D.C. Dunand: Acta Mater. 51 (2003) 4803.
[115] C.B. Fuller, J.L. Murray, D.N. Seidman: Acta Mater. 53 (2005) 5401.
[116] C.B. Fuller, D.N. Seidman: Acta Mater. 53 (2005) 5415.
[117] M.E. van Dalen, D.C. Dunand, D.N. Seidman: Acta Mater. 53 (2005) 4225.
[118] E.A. Marquis, D.N. Seidman: Acta Mater. 49 (2001) 1909.
[119] Y. Harada, D.C. Dunand: Mater. Sci. Eng. A 329 (2002) 686.
[120] Y. Harada, D.C. Dunand: Scripta Mater. 48 (2003) 219.
[121] J.L. Murray: Personal communication regarding the equilibrium Al–Ti phase diagram (2005).
[122] J.L. Murray, A. Peruzzi, J.P. Abriata: J. Phase Equil. 13 (1992) 277.
[123] T.W. Clyne, M.H. Robert: Met. Technol. 7 (1980) 177.
[124] P.D. Merica, R.G. Waltenberg, H. Scott: Scientific Papers of the Bureau of Standards 347 (1919) 271.
[125] N. Ryum, in: E.A. Starke, T.H. Sanders (Eds.), Aluminum Alloys: Their Physical and Mechanical Properties, Vol. 3. EMAS, Warley (1986) 1511.
[126] V.L. Kononenko, S.V. Golubev: Izv. Akad. Nauk. SSSR, Met. (1990) 197.
[127] V.L. Kononenko, S.V. Golubev: Russian Metall. (1990) 193.
[128] G. Rummel, T. Zumkley, M. Eggersmann, K. Freitag, H. Mehrer: Z. Metallkd. 86 (1995) 122.
[129] G. Rummel, T. Zumkley, M. Eggersmann, K. Freitag, H. Mehrer: Z. Metallkd. 86 (1995) 131.
[130] S.I. Fujikawa: J. Japan Inst. Light Metals 46 (1996) 202.
[131] Y. Du, Y.A. Chang, B. Huang, W. Gong, Z. Jin, H. Xu, Z. Yuan, Y. Liu, Y. He, F.Y. Xie: Mater. Sci. Eng. A 363 (2003) 140.
[132] J. Grammatikakis, K. Eftaxias, V. Hadjicontis: J. Phys. Chem. Solids 49 (1988) 1275.
[133] O. Madelung (Ed.): Landolt-Börnstein: Numerical Data and Functional Relationships in Science and Technology, Vol. 26 of Diffusion in Solid Metal. and Alloys. Springer-Verlag, Berlin (1990).
[134] S. Dais, R. Messer, A. Seeger: Mater Sci. Forum 15–18 (1987) 419.
[135] S.I. Fujikawa: Def. Diff. Forum 143–147 (1997) 115.
[136] D. Bergner, N. van Chi: Wissenschaftliche Zeitschrift der Pädagogischen Hochschule 15 (1977).
[137] G. Erdelyi, D.L. Beke, F.J. Kedves, I. Godeny: Phil. Mag. B 38 (1978) 445.
[138] S. Fujikawa, K. Hirano: Def. Diff. Forum 66–69 (1989) 447.
[139] N.L. Peterson, S.J. Rothman: Phys. Rev. B 1 (1970) 3264.
[140] T. Marumo, S. Fujikawa, K. Hirano: J. Japan Inst. Light Metals 23 (1873) 17.
[141] K. Hirano, S.I. Fujikawa: J. Nuc. Mater. 69–70 (1978) 564.
[142] N. van Chi, D. Bergner, in: F.J. Kedves, D.L. Beke (Eds.), DIMETA-82: Diffusion in Metals and Alloys. Trans Tech Publications, Switzerland (1983) 334.
[143] S.P. Murarka, R.P. Agarwala: Diffusion of rare earth elements in aluminum. Tech. Rep. 368, Bhabha Atomic Research Center (Indian Atomic Energy Commision) (1968).
[144] L.F. Mondolfo: Aluminum Alloys: Structure and Properties. Butterworths, London (1976).
[145] D. Lazarus: Phys. Rev. 93 (1954) 973.
[146] A.D. LeClaire: Phil. Mag. 7 (1962) 141.
[147] P. Shewmon: Diffusion in Solids. Second ed. The Minerals, Metals, and Materials Society, Warrendale, PA (1989).
[148] J. Philibert: Atomic Movements – Diffusion and Mass Transport in Solids. Monographies de physique. Les Editions de Physique, Les Ulis, France (1991).
[149] T. Hoshino, R. Zeller, P.H. Dederichs: Phys. Rev. B 53 (1996) 8971.
[150] W.B. Alexander, L.M. Slifkin: Phys. Rev. B 1 (1970) 3274.
[151] L.M. Angers, D.G. Konitzer, J.L. Murray, W.G. Truckner, in: Y.W. Kim, W.M. Griffith (Eds.), Dispersion Strengthened Aluminum Alloys. TMS (1988) 355.
[152] R.C. Weast, M.J. Astle, W.H. Beyer (Eds.): Handbook of Chemistry and Physics, 66th ed. CRC Press, Boca Raton (1985).
[153] F.A. Crossley, L.F. Mondolfo: Trans. AIME 191 (1951) 1143.
[154] D.G. McCartney: Int. Mater. Rev. 34 (1989) 247.
[155] B.S. Murty, S.A. Kori, M. Chakraborty: Int. Mater. Rev. 47 (2002) 3.
[156] J. Marcantonio, L.F. Mondolfo: J. Inst. Metals 98 (1970) 23.
[157] J. Marcantonio, L.J. Mondolfo: Metall. Trans. 2 (1971) 465.
[158] T. Ohashi, R. Ichikawa: Z. Metallkd. 64 (1973) 517.
[159] G.P. Jones, J. Pearson: Metall. Trans. B 7 (1976) 223.
[160] D.H.St. John, L.M. Hogan: J. Austral. Inst. of Metals 22 (1977) 160.
[161] L. Arnberg, L. Backerud, H. Klang: Met. Technol. 9 (1982) 1.
[162] L. Arnberg, L. Backerud, H. Klang: Met. Technol. 9 (1982) 7.
[163] L. Arnberg, L. Backerud, H. Klang: Met. Technol. 9 (1982) 14.
[164] G.K. Sigworth: Metall. Trans. A 15 (1984) 277.
[165] L. Bäckerud, G. Chai, J. Tamminen: Solidification Characteristics of Aluminum Alloys. Vol. 1. Wrought Alloys. American Foundrymen's Society (1990).
[166] K.T. Kashyap, T. Chandrashekar: B. Mater. Sci. 24 (2001) 345.

[167] H.W. Kerr, J. Cisse, G.F. Bolling: Acta Metall. 22 (1974) 677.
[168] H.W. Kerr, W. Kurz: Int. Mater. Rev. 41 (1996) 129.
[169] D.H.St. John, L.M. Hogan: J. Mater. Sci. 17 (1982) 2413.
[170] S.P. Midson, H. Jones, in: T. Masumoto, K. Suzuki (Eds.), Proc. 4th Int. Conf on Rapidly Quenched Metals, Vol. 2. The Japan Institute of Metals, Sendai, Japan (1981) 1539.
[171] N.J.E. Adkins, N. Saunders, P. Tsakiropoulos: Mater. Sci. Eng. 98 (1988) 217.
[172] B. Chalmers: Principles of Solidification. John Wiley & Sons, Inc., New York (1964).
[173] M.C. Flemings: Solidification Processing. McGraw-Hill, New York (1974).
[174] W. Kurz, D.J. Fisher: Fundamentals of Solidification. Fourth revised ed. Trans Tech Publications (1998).
[175] M.Y Drits, L.B. Ber, Y.G. Bykov, L.S. Toropova, G.K. Anastasyeva: Fiz. metal. metalloved. 57 (1984) 1172.
[176] C.B. Fuller, D.N. Seidman, D.C. Dunand: Scripta Mater. 40 (1999) 691.
[177] D.N. Seidman, E.A. Marquis, D.C. Dunand: Acta Mater. 50 (2002) 4021.
[178] E.A. Marquis, D.N. Seidman, D.C. Dunand: Acta Mater. 51 (2003) 4751.
[179] E.A. Marquis, D.N. Seidman: Acta Mater. 53 (2005) 4259.
[180] E.A. Marquis, D.N. Seidman, M. Asta, C. Woodward: Acta Mater. 54 (2006) 119.
[181] K.E. Knipling, D.C. Dunand, D.N. Seidman: Submitted to Scripta Mater (2006).
[182] S. Hori, S. Saji, T. Kobayashi: Technology Reports of the Osaka University 28 (1978) 359.
[183] S. Hori, S. Saji, T. Kobayashi: J. Japan Inst. Metals 37 (1973) 1134.
[184] R. Ichikawa, T. Ohashi: J. Japan Inst. Light Metals 18 (1968) 314.
[185] N. Ryum: J. Inst. Metals 94 (1966) 191.
[186] M. Sundberg, R. Sundberg, B. Jacobson: Jernkont. Ann. 155 (1971) 1.
[187] S. Rystad, N. Ryum: Aluminium 53 (1977) 193.
[188] H. Westengen, L. Auran, O. Reiso: Aluminium 57 (1981) 797.
[189] A. Ruder, D. Eliezer: Israel J. Tech. 24 (1988) 149.
[190] A. Ruder, D. Eliezer: J. Mater. Sci. 24 (1989) 1474.
[191] A. Ruder, D. Eliezer: J. Mater. Sci. Lett. 8 (1989) 725.
[192] G. Waterloo, H. Jones: J. Mater. Sci. 31 (1996) 2301.
[193] Z.G. Zhang, X.F. Bian, Y. Wang: Z. Metallkd. 93 (2002) 578.
[194] S.J. Savage, F.H. Froes, in: B.H. Kear, B.C. Giessen (Eds.), Rapidly Solidified Metastable Materials, Vol. 28. North-Holland, New York (1984) 329.
[195] D. Eliezer, S.J. Savage, Y.R. Mahajan, F.H. Froes, in: B.C. Giessen, D.E. Polk, A.I. Taub (Eds.), Rapidly Solidified Alloys and Their Mechanical and Magnetic Properties, Vol. 58. MRS, Pittsburgh (1986) 293.
[196] S.J. Savage, Y.R. Mahajan, A.G. Jackson, F.H. Froes, in: S. Steeb, H. Warlimont (Eds.), Rapidly Quenched Metals, Proceedings of the Fifth International Conference on Rapidly Quenched Metals, Würzburg, Elsevier Science Publishers (1985) 915.
[197] M. Fass, D. Itzhak, D. Eliezer, F.H. Froes: J. Mater. Sci. Lett. 6 (1987) 1227.
[198] M. Fass, D. Itzhak, D. Eliezer, F.H. Froes: J. Mater. Sci. Lett. 7 (1988) 76.
[199] A. Ruder, D. Eliezer: J. Mater. Sci. 25 (1990) 3541.
[200] Z. Nie, T. Jin, J. Fu, G. Xu, J. Yang, J. Zhou, T. Zuo, in: Aluminum Alloys 2002: Their Physical and Mechanical Properties Pts. 1–3, Vol. 396–402 of Materials Science Forum (2002) 1731.
[201] Z.R. Nie, T.N. Jin, J.X. Zou, J.B. Fu, J.J. Yang, T.Y. Zuo: Trans. Nonferrous Met. Soc. China 13 (2003) 509.
[202] Z.R. Nie, J.B. Fu, J.X. Zou, T.N. Jun, J.J. Yang, G.F. Xu, H.Q. Ruan, T.Y Zuo, in: J.F. Nie, A.J. Morton, B.C. Muddle (Eds.), Aluminium Alloys – Their Physical and Mechanical Properties, Vol. 28. Institute of Materials Engineering Australasia (2004) 197.

(Received October 21, 2005; accepted December 1, 2005)

Correspondence address

Prof. David N. Seidman
Department of Materials Science and Engineering
Northwestern University
2220 Campus Dr., Evanston, IL-60208-3108, USA
Tel.: +1 847 491 4391
Fax: +1 847 467 2269
E-mail: d-seidman@northwestern.edu